https://doi.org/10.5194/egusphere-2026-3543
Preprint. Discussion started: 6 July 2026

Enhanced warm-temperature marine ice-nucleating particles over the Arctic Ocean versus Asian-dust outflow at Jeju Island from real-time shipborne observations

Joo Wan Cha[1], Bu-Yo Kim[1], Miloslav Belorid[1], Young-Suk Oh[1], Myeonghun Kang[1], Seungbum Kim[1], Young Jun Yoon[2], Jiyeon Park[2], and Sang-Jong Park[2]

[1]National Institute of Meteorological Sciences (NIMS), Korea Meteorological Administration (KMA), Seogwipo, Republic of Korea
[2]Korea Polar Research Institute (KOPRI), Incheon, Republic of Korea

Correspondence: Joo Wan Cha (jwcha@korea.kr)

Abstract. Ice-nucleating particles (INPs) influence mixed-phase cloud microphysics and the Earth's radiative budget, yet observational records over the remote Arctic Ocean and contrasting continental-outflow environments remain sparse. This study presents INP concentrations measured by the Portable Ice Nucleation Experiment (PINE) over the Arctic Ocean during two RV(Research Vessel) Araon campaigns (ARA15A in 2024 and ARA16A in 2025) and at the Korea-Cloud Physics Experiment Chamber (K-CPEC) on Jeju Island, Korea (February–May 2024), totalling 41,524 expansion runs of which 35,370 passed rigorous quality control. INP temperature spectra differed markedly among the three datasets. At a representative warm temperature ($-20\,^{\circ}$C), median concentrations were 3.68 L^{-1} (ARA15A), 3.64 L^{-1} (ARA16A), and 0.89 L^{-1} at Jeju (Clean-day subset), with Arctic values exceeding Jeju; at a representative cold temperature ($-28\,^{\circ}$C), the pattern reversed — the Jeju Clean-day median rose to 8.22 L^{-1} while Arctic medians remained comparatively flat (ARA15A: 7.02 L^{-1}; ARA16A: 6.39 L^{-1}). Campaign-wide medians were comparable between the two Arctic years (6.83 and 6.57 L^{-1}) but differed approximately two-fold in the 75–80° N latitude band (ARA15A: 1.56 and ARA16A: 3.19 L^{-1}). These spectral contrasts are consistent with a marine biogenic-influenced regime at the Arctic warm-temperature end and an Asian-dust-influenced regime at the Jeju cold-temperature end, although direct compositional confirmation (heat treatment, chemical speciation) was not available in this dataset; all source attributions should therefore be interpreted as spectrally-consistent hypotheses rather than established source identifications. A dedicated ship-exhaust quality control scheme applied to both campaigns provides a replicable contamination-removal framework for future shipborne INP studies, and the combined dataset delivers new observational benchmarks for Arctic INP variability across the sampled 2024–2025 cruise periods.

Keywords. ice-nucleating particles, Arctic Ocean, Jeju Island, PINE instrument, shipborne measurements, ship exhaust quality control, marine biogenic aerosol, Asian dust, sea ice

https://doi.org/10.5194/egusphere-2026-3543
Preprint. Discussion started: 6 July 2026

1 Introduction

Ice-nucleating particles (INPs) play a pivotal role in the formation of ice crystals within mixed-phase clouds, thereby influencing precipitation initiation, cloud lifetime, and the Earth's radiative energy budget (DeMott et al., 2010; Murray et al., 2012). By lowering the energy barrier for freezing supercooled water droplets, INPs trigger the glaciation of clouds at temperatures substantially warmer than the homogeneous freezing threshold ($\sim -38\,^{\circ}\mathrm{C}$). The resulting change in cloud phase significantly alters the optical properties and precipitation efficiency of cloud systems, with implications for both regional weather and global climate sensitivity (Kanji et al., 2017). Secondary ice processes, which amplify primary heterogeneous ice formation in mixed-phase clouds, further complicate the link between INP abundance and cloud glaciation (Pasquier et al., 2022). The Arctic region is particularly sensitive to these microphysical processes because mixed-phase clouds are ubiquitous throughout the year and exert a disproportionate influence on the surface energy balance (Kanji et al., 2017). Arctic amplification — the observed warming of the Arctic at roughly two to four times the global mean rate — is thought to be modulated in part by cloud–ice feedbacks, yet the representation of these feedbacks in climate models remains highly uncertain (Murray et al., 2012). Satellite-constrained model experiments demonstrate that correcting the underestimated supercooled liquid fraction in mixed-phase clouds substantially alters Arctic amplification through changes in downward longwave radiation trapped at the surface under the region's unique stable stratification conditions (Tan and Storelvmo, 2019); the direction and magnitude of this response depend critically on the abundance and efficiency of INP, which control the liquid-to-ice partitioning in these clouds. Reducing this uncertainty requires improved observational constraints on INP concentrations and sources across the Arctic, which are currently sparse relative to mid-latitude and tropical environments (DeMott et al., 2010; Schmale et al., 2021; Willis et al., 2018).

Despite growing recognition of their importance, INP observations over the Arctic Ocean remain limited in both spatial coverage and temporal continuity. Shipborne and airborne campaigns have provided valuable but geographically constrained datasets; for example, Irish et al. (2019) reported INP concentrations in surface seawater and the overlying marine boundary layer in the Canadian Arctic, and Creamean et al. (2018) characterised INP abundance and sources during a trans-Arctic voyage. Ground-based measurements at high-latitude stations have complemented these efforts (Wex et al., 2019; Hartmann et al., 2021; Creamean et al., 2019; Säntl-Temkiv et al., 2019), and episodic high-latitude dust source contributions — notably from Iceland — have been shown to generate mixed-phase-cloud-relevant INP populations (Sanchez-Marroquin et al., 2020), yet systematic surveys of the INP spatial distribution across the broader Arctic Ocean — particularly spanning multiple years and seasons — are still lacking. The contribution of marine biogenic material, including sea-spray-associated organic matter and phytoplankton-derived exudates, to Arctic INP populations remains poorly constrained (DeMott et al., 2016; McCluskey et al., 2018; Porter et al., 2022), hampering source attribution and model parameterisation. An additional practical challenge in shipborne INP observations is contamination by ship-exhaust aerosols: combustion emissions from the vessel's own engines can produce transient INP concentration spikes that, if undetected, introduce substantial positive biases into the observational record. Robust quality-control methodologies to identify and remove such pollution events are therefore an essential prerequisite for reliable open-ocean INP datasets.

https://doi.org/10.5194/egusphere-2026-3543
Preprint. Discussion started: 6 July 2026

In contrast to the high-latitude marine environment, the INP characteristics of East Asian outflow have been shaped by a different set of sources, dominated by mineral dust mobilised from the arid regions of the Asian continent and by anthropogenic aerosols associated with rapid industrialisation. Jeju Island, situated in the northern East China Sea, serves as a sentinel site for monitoring trans-boundary transport of dust and pollution aerosols from China and the Korean Peninsula (Iwata and Matsuki, 2018; Chen et al., 2018). Springtime Asian dust (*hwangsa*) events, which regularly affect the Korean Peninsula and surrounding seas between February and May, have been shown to elevate INP concentrations by one to several orders of magnitude relative to background conditions (Iwata and Matsuki, 2018; Chen et al., 2018; Tobo et al., 2019). Although these dust-dominated INP enhancements are well documented in laboratory studies of mineral dust ice nucleation efficiency, long-term continuous observational records from ground-based sites in the East Asian outflow region remain scarce, and the relative contributions of mineral dust versus anthropogenic or biogenic aerosols at temperatures below approximately $-20\,^{\circ}\mathrm{C}$ are not fully resolved (Iwata and Matsuki, 2018). Furthermore, direct comparison between INP properties measured at a continental-outflow receptor site such as Jeju and those measured over the remote Arctic Ocean — where marine biogenic sources are thought to play a more prominent role at warmer supercooling temperatures (DeMott et al., 2016; McCluskey et al., 2018; Wilson et al., 2015) — has not previously been reported, limiting understanding of how source region influences INP temperature spectra.

This study presents INP observations collected with the online PINE (Portable Ice Nucleation Experiment) instrument, which enables continuous, high-temporal-resolution measurements of INP number concentrations across a temperature range of -15 to $-33\,^{\circ}\mathrm{C}$. To our knowledge, this represents the first deployment of an online expansion-chamber INP instrument over the Arctic Ocean: previous shipborne Arctic Ocean INP records rely on offline filter assays (Porter et al., 2022; Creamean et al., 2022) or, for the cold-temperature range, online continuous-flow diffusion chambers (Li et al., 2025), leaving the warm-temperature (-15 to $-22\,^{\circ}\mathrm{C}$) marine regime comparatively undersampled at high temporal resolution. Observations were obtained during two Arctic expeditions aboard the Korean icebreaker RV Araon (ARA15A in 2024 and ARA16A in 2025) and at the ground-based K-CPEC supersite on Jeju Island from February to May 2024, encompassing multiple springtime dust episodes. We hypothesise that source region, rather than latitude alone, influences the shape of the INP temperature spectrum, with marine biogenic emissions making a more prominent contribution to Arctic populations at warmer temperatures (-15 to $-22\,^{\circ}\mathrm{C}$) and mineral dust from Asian continental outflow contributing more strongly at colder temperatures ($\leq -25\,^{\circ}\mathrm{C}$); we further hypothesise (as an exploratory question only) that recent sea-ice retreat may co-vary with biogenic INP emissions over the open Arctic Ocean. The latter relationship is examined as an observational association in this study and cannot be evaluated causally without additional process-level measurements. Four objectives are addressed. First, the spatial distribution of INP concentrations across the Arctic Ocean is characterised using the two multi-year shipborne datasets, providing the first systematic survey of Arctic INP variability spanning both the 2024 and 2025 summer seasons. Second, the INP temperature spectra observed over the Arctic Ocean are compared with those at the Jeju continental-outflow site to examine the potential differing contributions of marine biogenic and mineral dust sources. Third, a ship-exhaust contamination identification and removal methodology is developed and applied to both shipborne datasets (ARA15A and ARA16A), offering a replicable quality-control framework for future shipborne INP studies. Fourth, as an exploratory extension, the relationship between

https://doi.org/10.5194/egusphere-2026-3543
Preprint. Discussion started: 6 July 2026

pan-Arctic sea-ice retreat, satellite-derived chlorophyll-a, and observed INP concentrations is examined across the 2024–2025 Arctic record to evaluate the plausibility of a sea-ice–biology–INP linkage.

The present study makes four specific contributions to the observational and methodological record: (1) it provides the first systematic multi-year shipborne PINE dataset from the same vessel and route in consecutive Arctic summers (2024 and 2025), enabling direct year-on-year comparison of Arctic INP variability with a controlled observing platform; (2) it presents a replicable two-phase ship-exhaust quality control framework with documented sensitivity analysis (Sect. 2.5.2, Table S3 in the Supplement), directly transferable to future online shipborne INP campaigns; (3) it derives a literature-justified fixed correction factor (CF $= 16$, defined as the median PINE/Filter concentration ratio at $T = -20\,^{\circ}$C; PINE concentrations are divided by CF to place them on the Filter-equivalent scale; Appendix A) enabling PINE-measured INP concentrations to be placed, for first-order order-of-magnitude comparison, on the same scale as established filter-based Arctic datasets; and (4) the combined ARA15A/ARA16A dataset, together with the co-located Jeju observations, provides observational benchmarks at $T = -20$ to $-25\,^{\circ}$C suitable for evaluating the marine biogenic INP parameterisations used in atmospheric model frameworks such as the National Center for Atmospheric Research (NCAR) Community Atmosphere Model version 6 (CAM6) and EC-Earth (Tan et al., 2016; Shi and Liu, 2019).

2 Methods

2.1 PINE instrument and measurement principle

The Particle Ice Nucleation Experiment (PINE) instrument, developed at Bilfinger Noell GmbH (Germany), was used to measure ice nucleating particle (INP) concentrations in this study (Möhler et al., 2021; Böhmländer et al., 2025). PINE detects INPs through adiabatic expansion cooling: a sample of ambient air (∼1.8–2.0 L per expansion cycle) is rapidly cooled within a stainless-steel expansion chamber to a target temperature, and ice crystals nucleated during the expansion are counted by an integrated POPS (Printed Optical Particle Spectrometer) optical particle counter. The instrument covers a temperature range of -10 to $-65\,^{\circ}$C; in the present study, measurements were conducted across a temperature range of approximately -15 to $-33\,^{\circ}$C; runs with a minimum chamber temperature $> -15\,^{\circ}$C were excluded from the analysis dataset, as were instrument warm-up expansions at the start of each operation (typically the first 1–5 runs) which do not yet reach the target heterogeneous-freezing regime. PINE was operated in temperature-ramp mode for both the K-CPEC ground-based (PINE-06-03) and ARAON shipborne (PINE-06-02) deployments. Each measurement cycle comprised a sample flush phase (130–160 s at flow 1.0–1.5 stdL min^{-1}) at ambient pressure, a rapid adiabatic expansion phase (∼30–40 s at flow 3.0 stdL min^{-1}) cooling the chamber to the target temperature setpoint, and a refill/recovery phase (∼50–120 s) returning the chamber to ambient conditions, yielding a total cycle duration of approximately 4–5 min (run-to-run interval 244–300 s). The target chamber temperature was ramped progressively across the operational -15 to $-33\,^{\circ}$C range, with INP concentrations aggregated into 0.5 °C temperature bins for L2 spectral products (Sect. 2.6). The K-CPEC cycle (∼4 min: 158 s flush, ∼30 s expansion, ∼49 s refill) was slightly shorter than the ARAON cycle (∼5 min: 130 s flush, ∼39 s expansion, ∼121 s refill), reflecting deployment-specific operational tuning; per-operation cycle parameters are archived under “Data availability”. INP number concentrations are derived from ice crystal

https://doi.org/10.5194/egusphere-2026-3543
Preprint. Discussion started: 6 July 2026

counts and sampled air volume using the onboard PINE Inversion Algorithm (PIA, v3.1.0). All concentrations are internally referenced to standard conditions (0 °C, 1013.25 hPa) and are therefore expressed in standard litres (stdL^{-1}); for conciseness, this unit is abbreviated as L^{-1} throughout the text. The difference between ambient and standard volumes is $\leq 4\,\%$ under the conditions of this study, following the standard-conditions framework adopted in the PIA inversion code (Möhler et al., 2021); this correction is negligible relative to other measurement uncertainties. PINE counting performance has been characterised against reference INP counters in previous deployments and chamber intercomparisons, with PINE agreeing within a factor of $\sim$2–5 across the majority of co-located methods evaluated (Vepuri et al., 2021; DeMott et al., 2018; Lacher et al., 2024); the detailed PICNIC intercomparison statistics are revisited in Sect. 4.4.

2.2 Observation campaigns

2.2.1 Jeju Island — K-CPEC site (February–May 2024)

Ground-based INP observations were conducted using the PINE instrument at the Korea-Cloud Physics Experiment Chamber (K-CPEC) site on Jeju Island, South Korea (33.3° N, 126.6° E, 75 m a.s.l.) from February to May 2024, encompassing the spring Asian dust season. The PINE instrument sampled near-surface ambient air continuously over 20 individual daily measurement campaigns, yielding a total of 18,350 expansion runs across 20 individual measurement operations, of which 12,196 (66.5 %) passed all automated quality checks (see Sect. 2.5.1 for the run-exclusion breakdown). Air masses were classified into three categories based on monitoring of particulate matter with aerodynamic diameter $\leq 10\,\mu$m (PM_{10}) at the Gosan background station (33.3° N, 126.2° E, 72 m a.s.l.; AirKorea 2024) and synoptic meteorological analysis: (1) **Clean Marine** (5 March 2024): PM_{10} daily mean of 4 μg m^{-3} (max. 9 μg m^{-3}), with westerly to north-westerly flow originating from the open North Pacific; (2) **Polluted** (2–3 March 2024): PM_{10} daily means of 23 and 61 μg m^{-3} on 2 and 3 March, respectively (peak hourly value: 72 μg m^{-3}), with air masses transiting the Korean Peninsula or eastern China under southwesterly synoptic flow; and (3) **Asian Dust** (18–19 March 2024): PM_{10} hourly peaks of 102 and 238 μg m^{-3} on 18 and 19 March, respectively, during confirmed dust transport events, consistent with northwesterly continental outflow from the Gobi or Taklamakan deserts.

2.2.2 Arctic Ocean — RV Araon ARA15A (July–September 2024)

Shipborne INP measurements were carried out aboard the Korean icebreaker RV Araon (KOPRI, 7,487 t) during the 2024 Arctic expedition ARA15A. The vessel sailed from Incheon, South Korea, northward through the Bering Sea and Chukchi Sea to the central Arctic Ocean, reaching a maximum latitude of approximately 80° N. Observations were made during summer (July–September 2024) across 4 measurement operations (11–12 July 2024, 12–28 July 2024, 31 July – 14 August 2024, and 14–25 August 2024), producing 11,854 valid Level 1 (L1) expansion runs in total. The PINE instrument was installed on the forward section of the ship's main deck to minimise exhaust contamination(Table S1 in the Supplement).

https://doi.org/10.5194/egusphere-2026-3543
Preprint. Discussion started: 6 July 2026

2.2.3 Arctic Ocean — RV Araon ARA16A (July–September 2025)

A second Arctic shipborne campaign was conducted during the ARA16A expedition from July to September 2025, following a route from South Korea through the North Pacific, Bering Sea, Chukchi Sea, and into the Beaufort Sea, again reaching ∼80° N. Measurements were organised into 19 individual operations. This campaign included dedicated ship-contamination quality control (QC) procedures (described in Sect. 2.5.2): eight operations within or immediately preceding the inlet malfunction period (11 July – 7 August 2025) were fully excluded (including one aborted 102-second initialisation session with no data; Table S2 in the Supplement), while one further operation (6–12 August 2025) fell partially within this period but yielded valid measurements from 8–12 August after the inlet was restored. A further four operations were excluded due to absent POPS data, leaving seven operations from which INP data were retrieved (Table S2 in the Supplement). Of these seven, the 8–12 August 2025 period passed run-level ship-contamination QC without spike removal; five operations were flagged as ship-exhaust-contaminated and subjected to run-level spike removal; and one (5–6 September 2025) was fully clean. The 11,320 L1 expansion runs reported for ARA16A correspond to the union of (i) 991 runs from 8–12 August 2025 passing ship-contamination QC, (ii) 1,548 runs from the clean operation 5–6 September 2025 retained without spike filtering, and (iii) 8,781 runs surviving run-level spike removal across the five partially-contaminated operations. Further details of the operation-level quality control are given in Sect. 2.5.2 and Sect. 3.4.

2.3 Auxiliary measurements

Aerosol particle number concentrations of particles with optical diameter $> 0.5\,\mu$m ($N_{>0.5}$, units: cm^{-3}) were recorded continuously by the POPS optical particle counter integrated within the PINE instrument; these data were used to support INP parameterisation comparisons following DeMott et al. (2010). For the shipborne campaigns, vessel position was logged at 1-minute intervals via the onboard DADIS (Data Acquisition and Display System) navigation system using GPS. For both Arctic campaigns (ARA15A 2024 and ARA16A 2025), high-resolution GPS navigation data recorded at 1-second intervals were available, providing course over ground (COG) and speed over ground (SOG) alongside the standard position record. These datasets were used in conjunction with heading information from ship-mounted instruments to compute the relative wind direction required for ship contamination screening (detailed in Sect. 2.5.2). Meteorological parameters including wind speed, wind direction, air temperature, and relative humidity were measured at 1-minute resolution by the ship's meteorological sensors.

2.4 Satellite-derived environmental data

To contextualise the shipborne INP observations within the broader Arctic marine environment, daily satellite-derived chlorophyll-a (Chl-a) and sea-ice concentration (SIC) data were obtained from the Copernicus Marine Service (CMEMS, https://marine.copernicus.eu/). Chl-a concentrations were derived from the Arctic Ocean multi-sensor L3 daily products (dataset IDs: `cmems_obs-oc_arc_bgc-plankton_my_l3-multi-4km_P1D` for 2024 and `cmems_obs-oc_arc_bgc-plankton_nrt_l3-multi-4km_P1D` for 2025) at 4 km horizontal resolution. Sea-ice concentration was extracted from the Arctic

https://doi.org/10.5194/egusphere-2026-3543
Preprint. Discussion started: 6 July 2026

Ocean Physics Analysis and Forecast product (`cmems_mod_arc_phy_anfc_6km_detided_P1D-m`) at 6 km resolution.

Environmental variables were spatially averaged over the central Arctic Ocean (defined as latitudes $\geq 70^\circ$ N) for the months of August and September in 2024 and 2025, matching the RV Araon campaign periods. Total Sea Ice Area (SIA, km^2) was calculated by integrating the fractional SIC over the central Arctic grid cells. These satellite-derived metrics were used to investigate the statistical relationship between marine primary productivity, sea-ice retreat, and atmospheric INP concentrations.

2.5 Quality control procedures

2.5.1 PIA v3.1.0 automated quality control

Raw PINE data (L0) were processed to quality-controlled INP concentrations (L1) using the PIA v3.1.0 software. Automated flagging criteria included checks on run mode (expansion type identifier), temperature stability during the cooling phase, and expansion pressure range; runs failing any of these checks were excluded from further analysis. Multi-level flags were assigned following a SaQC-based scheme, with separate flags applied for runs in which the ice crystal fraction (F_e) or the maximum ice fraction (F_m) fell outside their respective valid ranges. Only runs passing all automated quality gates were retained for statistical analysis.

For the Jeju 2024 dataset, 6,154 of the 18,350 expansion runs (33.5 %) were excluded following a two-tier protocol. First, three complete measurement operations were rejected at the operation level (totalling 1,458 runs; 23.7 % of all excluded runs): one on 9 May (instrument initialisation anomaly; 3 runs), one on 10 May (insufficient chamber cooling; 25 runs), and one on 28 February (inlet instability throughout the operation; 1,430 runs). Second, the remaining 4,696 excluded runs (76.3 % of excluded total) were flagged individually by the PIA automated system. Analysis of the per-run QC flag logs identified the following primary causes, listed in decreasing order of frequency: (i) insufficient ice supersaturation at the start of expansion, indicating that the chamber did not reach the required supercooled state, accounting for approximately 36 % of run-level exclusions and disproportionately affecting short measurement periods with warm ambient conditions; (ii) ice carry-over from the previous expansion cycle, detected as a non-zero ice crystal fraction ($F_e \neq 0$) during the flush phase ($\sim$15 %); (iii) particle contamination detected during the chamber refill phase ($\sim$15 %); (iv) temperature sensor readings outside the valid range during flush or refill ($\sim$11 %); (v) statistical outliers in the maximum ice fraction F_m ($\sim$6 %); and (vi) remaining causes including ice threshold anomalies and dewpoint sensor exceedances ($\sim$17 %). The elevated exclusion rate during the February–March campaigns (40–75 % per operation) reflects the high aerosol loading and frequent chamber saturation events under Asian dust conditions, whereas the May operations showed substantially lower exclusion rates (10–18 %).

2.5.2 Ship contamination (spike) identification and removal

Because ship exhaust can substantially elevate apparent INP concentrations during shipborne measurements, a dedicated spike-removal procedure was applied to both the ARA15A and ARA16A shipborne datasets. The quality control scheme is illustrated in Fig. 1. A run was flagged as contaminated if it met any one of the following criteria: (1) the corrected relative wind direction

https://doi.org/10.5194/egusphere-2026-3543
Preprint. Discussion started: 6 July 2026

at the inlet fell within the stern sector (135–225°), indicating possible exhaust entrainment from the aft funnel (Modini et al., 2015); (2) the relative wind speed at the inlet (WS_r) fell below 2.0 m s^{-1}, a stagnant-air condition under which engine exhaust can accumulate around the hull and be advected to the inlet irrespective of nominal wind direction (Tatzelt et al., 2022); (3) the single-run INP concentration exceeded 100 times the rolling 60-minute median of runs passing criteria (1)–(2) within the same operation (hereafter the *local background*), targeting transient exhaust plume breakthrough events; or (4) the INP concentration exceeded 200 L^{-1} at temperatures warmer than −19 °C. The −19 °C / 200 L^{-1} pair corresponds approximately to the 99.5th percentile of clean-period INP across the three campaigns and marks the regime in which contamination events become readily distinguishable from natural aerosol loading in the high-latitude boundary layer; the sensitivity of the derived INP statistics to ±50 % perturbations of this and the other thresholds is evaluated in Supplement Table S3 and yields < 5 % change in campaign-median INP. Relative wind direction (WD_r) and speed (WS_r) were computed from measured true wind direction (WD_t) and vessel heading (HDG) as $WD_r = WD_t - HDG \pmod{360°}$. For ARA15A 2024, heading was obtained directly from the RV Araon shipboard automatic weather station (AWS; Campbell Scientific CR3000 data logger, recording true wind and heading at 1-min resolution). For ARA16A 2025, course over ground (COG) from the GPS dataset (Sect. 2.3) was used as a heading proxy. During periods with SOG < 0.5 m s^{-1}, WD_r was set to undefined (not applied in criterion (1)) when COG is directionally unstable. Both campaigns employed relative wind measurements for contamination screening (criterion (2)); clean operations were defined as those in which none of the contamination criteria were triggered and wind direction was confirmed from forward of the beam. Applying these filters to the full set of 19 operations first excluded 8 operations during the inlet malfunction period (11 July – 7 August 2025; including one aborted initialisation session; Table S2 in the Supplement); one further operation (6–12 August 2025) fell partially within this period but yielded valid data from 8–12 August after inlet restoration. A further 4 operations with absent POPS data were excluded, leaving 7 operations (8–12 August 2025, 13–17 August 2025, 17–19 August 2025, 19–22 August 2025, 24 August – 5 September 2025, 5–6 September 2025, and 6–21 September 2025; see Table S2 in the Supplement) suitable for geophysical interpretation.

Applying the dual-criterion filter to the matched wind-PINE dataset yields quantitative removal statistics: for ARA15A 2024, 705 of 6,261 wind-matched runs were flagged as contaminated (11.3 %; wind-direction criterion: 561 runs, 9.0 %; low-wind criterion: 144 additional runs, 2.3 %), leaving 5,556 clean runs (88.7 %) for geophysical analysis. For ARA16A 2025, only 128 of 6,138 runs were flagged (2.1 %; wind-direction: 113 runs; low-wind: 15 additional), leaving 6,010 clean runs (97.9 %). The lower contamination rate in ARA16A reflects the more favourable PINE inlet position (port bow, 02 Deck) relative to ARA15A (forward main deck), which reduced the fraction of time the stern sector was upwind of the inlet. To assess residual contamination, we compared INP distributions in sectors immediately adjacent to the stern zone (90–135° and 225–270°) against the clean forward sector (315–45°) using Mann–Whitney U tests; no statistically significant elevation was detected in either adjacent sector for ARA15A 2024 (both $p > 0.05$), indicating that spillover contamination from the stern zone was not a systematic feature of the retained dataset.

https://doi.org/10.5194/egusphere-2026-3543
Preprint. Discussion started: 6 July 2026

2.6 Data analysis and statistical methods

To enable scientifically consistent comparisons between the high-resolution PINE observations (2024–2025) and historical offline filter-based datasets (e.g., Wex et al. 2019; Creamean et al. 2022), a multi-step data integration and normalisation procedure was employed.

First, to address the discrepancy in sampling volumes and durations, PINE's expansion cycles were time-resampled to match the typical integrated periods of filter studies (e.g., 24-hour daily averages). For each resampled interval, the limit of detection (LOD) was calculated from a Poisson 95 % upper-confidence bound for zero observed counts:

$$LOD = \frac{3.0}{V_{total}} \tag{1}$$

where V_{total} is the sum of sampled air volumes [L] across all valid expansion cycles within the period; the constant 3.0 is the 95 % Poisson upper confidence limit when zero ice crystals are observed ($\chi^2_{2,\,0.95}/2 \approx 2.996$). Measurements falling below this LOD were excluded from the climatological trend analysis to ensure high data fidelity.

Second, a fixed empirical correction factor (CF $= 16$; derived and justified in Sect. 4.4 and Appendix A) was used to place the high-resolution PINE concentrations on the same scale as established offline filter-based Arctic datasets for first-order, order-of-magnitude comparison.

Third, we assessed the sensitivity of INP concentrations to a potential temperature offset (ΔT) arising from the difference between the PINE gas-phase temperature sensor reading and the actual temperature of cloud droplets during adiabatic expansion (Möhler et al., 2021). To quantify this effect for our datasets, we compared PINE Level-1 ice-file temperatures with Level-2 binned Temp_Spec temperatures across all three campaigns. The resulting mean offset was 0.02 ± 0.03 K across $N = 34{,}379$ paired Level 1 / Level 2 (L1/L2) runs, consistent with bin-averaging effects within the processing pipeline; this internal consistency check cannot rule out a physical gas–droplet temperature offset but demonstrates that no additional systematic bias is introduced by the post-processing binning (Fig. S1 in the Supplement). We additionally characterised the temperature sensitivity of INP concentrations as $\beta = \mathrm{d}\log_{10}(\mathrm{INP})/\mathrm{d}T$, obtaining $\beta = -0.022\,\mathrm{K}^{-1}$ for both Arctic campaigns (ARA15A and ARA16A) and $\beta = -0.081\,\mathrm{K}^{-1}$ for Jeju. Propagating the worst-case literature estimate of $\Delta T = 1.0$ K (Möhler et al., 2021) through these slopes yields INP concentration changes of $\approx -5\,\%$ for the Arctic datasets and $\approx -17\,\%$ for Jeju. No explicit ΔT correction was applied to the reported concentrations. The $-5\,\%$ Arctic impact is smaller than the fixed-CF uncertainty (factor of $\sim$2; Appendix A); for Jeju, the $-17\,\%$ impact, while not negligible for absolute values, does not affect the spectral shape comparisons or the sign of inter-campaign differences discussed in this study (Fig. S1 in the Supplement).

2.7 Multi-dataset monthly sea-ice synthesis

To place the ARAON (the operational call-sign of the Korean icebreaker RV *Araon*, hereafter used as the campaign-family identifier) observations in a longer-term context, we assembled a multi-dataset monthly synthesis spanning 2012–2025. Published Arctic INP concentrations at $T = -20\,^{\circ}$C were extracted from the literature (Supplement Table S4) and compared at the $T = -20\,^{\circ}$C reference temperature, where method-specific online–offline offsets are smallest (Sect. 4.4). The method-specific

https://doi.org/10.5194/egusphere-2026-3543
Preprint. Discussion started: 6 July 2026

multiplicative factors tabulated in Appendix A (Filter Ice Spectrometer (Filter IS) and DRoplet Ice Nuclei Counter Zurich (DRINCZ; David et al. 2019) $\times 7$ and $\times 61$ respectively; TROPOS-network filter-based immersion-freezing droplet assays at Arctic stations (hereafter Filter-imm; data from Wex et al. 2019; Hartmann et al. 2021; Sze et al. 2023) $\times 11.2$; PINE $\times 1$ as reference; and the Davis Rotating Unit for Monitoring (DRUM) cascade impactor dataset excluded) characterise the order-of-magnitude harmonisation framework, and the offline Filter-imm subset is harmonised to the PINE scale ($\times 11.2$) in the regression below. The full sensitivity of the regression to this factor (Filter-imm CF from $\times 1$, CF-naive, to $\times 47$) is documented in Supplement Fig. S7 and Table S9. The harmonised monthly INP values were paired with the corresponding monthly mean Arctic Sea Ice Extent (SIE, 10^6 km^2) from the National Snow and Ice Data Center (NSIDC) Sea Ice Index (National Snow and Ice Data Center (NSIDC), 2024, 2025). To remove the dominant intra-annual seasonal cycle that would otherwise induce spurious correlations, monthly SIE values were deseasonalised by subtracting the 1981–2010 monthly climatology, yielding SIE anomalies.

A log-linear regression of the form $\log_{10}(\mathrm{INP}) = a \cdot \mathrm{SIE}_{\mathrm{anom}} + b$ was fitted by ordinary least squares (OLS) in $\log_{10}$ space. Slope significance and its 95 % confidence interval were assessed using Newey–West heteroskedasticity- and autocorrelation-consistent (HAC) inference (Newey and West, 1987) to account for temporal autocorrelation in the monthly series. The Spearman rank correlation coefficient was computed in $\log_{10}$ space as a distribution-free measure of monotonic association. The 95 % bootstrap confidence band shown in Fig. 6b was constructed by computing, at each SIE anomaly value, the 2.5th and 97.5th percentiles of the 5,000 bootstrap-predicted $\log_{10}$ INP values and back-transforming to linear units.

HAC lag-selection details and residual autocorrelation diagnostics for the year-ordered monthly panel are reported in Supplement Table S7. Given the multi-dataset, multi-method composition of the synthesis, the resulting association is framed throughout as exploratory rather than diagnostic (Sect. 3.6).

3 Results

3.1 Overview of INP concentrations

A total of 41,524 PINE instrument runs were collected across three field deployments: Jeju 2024 ($n = 18{,}350$; 20 operations), Arctic 2024 (ARA15A; $n = 11{,}854$; 4 operations), and Arctic 2025 (ARA16A; $n = 11{,}320$; 7 operations) (Table 1). INP concentrations spanned several orders of magnitude within each dataset; the overall range was 0.52–1,022 L^{-1} at Jeju, 0.50–394 L^{-1} in Arctic 2024, and 0.50–311 L^{-1} in Arctic 2025 (Table 1). Because the distributions were strongly right-skewed, median and $\log_{10}$-transformed statistics are reported as primary descriptors.

To assess whether the two Arctic campaigns differ statistically at the run level, non-parametric Mann–Whitney U tests were applied at three representative temperatures: $-19.25\,^{\circ}$C, $-22.25\,^{\circ}$C, and $-25.25\,^{\circ}$C. The tests yielded $U = 6{,}927$ ($p = 0.826$), $U = 3{,}068$ ($p = 0.255$), and $U = 18{,}581$ ($p = 0.355$), respectively, with none surviving Benjamini–Hochberg false-discovery-rate correction at $\alpha = 0.05$. Bootstrap 95 % confidence intervals (5,000 resamples, $\log_{10}$ space, back-transformed) for the per-half-degree-bin medians are summarised in the Supplement (with the full per-bin table in the data archive) and are consistent with overlapping distributions at all temperatures: the overlapping CIs indicate that the run-level central tendencies of the two

https://doi.org/10.5194/egusphere-2026-3543
Preprint. Discussion started: 6 July 2026

Table 1. Summary of PINE measurement campaigns and quality-controlled run statistics for the three field deployments.

Campaign	Period	Location	Ops (Valid/Total)	No. Runs (QC'd)	Valid Cases	Valid (%)[a]
ARAON 2024 (ARA15A)	Jul–Sep 2024	Arctic Ocean	4 / 4	11,854	11,854	100.0
ARAON 2025 (ARA16A)	Jul–Sep 2025	Arctic Ocean	7 / 19[b]	11,320	11,320	100.0[c]
Jeju 2024	Feb–May 2024	Jeju Island, Korea	20 / 20	18,350	12,196	66.5
Total			31 / 43	41,524	35,370	85.2

[a] Valid (%) = Valid Cases / No. Runs (QC'd) × 100. For ARA16A 2025, computed within the seven valid operations only (see note [c]).

[b] 12 operations excluded: 8 fully during the inlet malfunction period (11 Jul – 7 Aug 2025; incl. one aborted session) and 4 with absent POPS data; one inlet-period operation (6–12 Aug) contributed valid data from 8–12 Aug after inlet restoration.

[c] 100.0 % denotes full retention of runs within the seven valid operations; the 12 excluded operations are not reflected in this percentage.

campaigns are statistically indistinguishable, notwithstanding their approximately two-fold difference at the latitude-resolved 75–80° N band (Sect. 3.3). This result reinforces the caution from Sect. 4.3 that per-run n overstates statistical degrees of freedom; the apparent latitude-band contrast is more appropriately interpreted at the operation or segment level.

In Table 1, "Ops (Valid/Total)" denotes operations retained for analysis out of all conducted; "No. Runs (QC'd)" is the expansion run count from valid operations after all QC stages; and "Valid Cases" are runs additionally passing all automated PIA quality flags. For Jeju 2024, all 20 operations were retained and run-level PIA QC excluded 6,154 of 18,350 runs (33.5 %; Sect. 2.5.1). For Arctic 2024 (ARA15A), all 4 operations passed ship-contamination screening with no additional run-level exclusions, so the run count equals the valid count; the full operation-level QC log is provided in Supplement Table S1. For Arctic 2025 (ARA16A), 12 of 19 operations were excluded at the operation level (Sect. 2.5.2), leaving 7 operations from which 991 clean runs (8–12 August), 1,548 fully clean runs (5–6 September), and 8,781 spike-filtered runs were retained; the Valid (%) of 100.0 % reflects retention within these seven valid operations only. A full operation-level QC log for ARA16A 2025 is provided in Supplement Table S2.

The campaign-wide median INP concentration (aggregated across all measured temperatures, -15 to $-33\,^{\circ}$C) was highest at Jeju (8.02 L^{-1}; interquartile range [IQR]: 2.22–24.3 L^{-1}), intermediate in Arctic 2024 (6.83 [3.55–10.75] L^{-1}), and similar in Arctic 2025 (6.57 [3.49–6.98] L^{-1}), while the arithmetic means were substantially elevated relative to the medians in the Jeju dataset and more moderate in the Arctic datasets (22.9, 9.62, and 6.40 L^{-1}, respectively), reflecting the influence of sporadic high-concentration events (Fig. 2). The $\log_{10}$-mean $\pm$ standard deviation ($\log_{10} L^{-1}$) was 0.89 ± 0.67 for Jeju, 0.856 ± 0.302 for Arctic 2024, and 0.741 ± 0.214 for Arctic 2025, indicating comparable logarithmic variability across sites despite differing central tendencies. In log space, comparable standard deviations imply similar relative variability: each site's INP concentrations fluctuate by comparable multiplicative factors around their respective central values, meaning that although absolute concentrations differ, the fractional variability (as a percentage or multiplicative spread) is similar across all three regions.

https://doi.org/10.5194/egusphere-2026-3543
Preprint. Discussion started: 6 July 2026

Table 2. Temperature-bin median INP concentrations (L^{-1}) at key temperatures.

Campaign / Category	$T = -19\,°C$	$T = -20\,°C$	$T = -22\,°C$	$T = -25\,°C$	$T = -28\,°C$
ARAON 2024 (ARA15A)	3.58 ($n = 111$)	3.68 ($n = 173$)	3.67 ($n = 94$)	3.66 ($n = 383$)	7.02 ($n = 875$)
ARAON 2025 (ARA16A)	6.75 ($n = 427$)	3.64 ($n = 593$)	6.20 ($n = 271$)	6.49 ($n = 297$)	6.39 ($n = 612$)
Jeju — Clean	0.51 ($n = 14$)	0.89 ($n = 14$)	1.25 ($n = 61$)	4.32 ($n = 11$)	8.22 ($n = 12$)
Jeju — Polluted	1.93 ($n = 22$)	3.74 ($n = 22$)	9.07 ($n = 143$)	19.20 ($n = 22$)	38.48 ($n = 25$)
Jeju — Asian Dust	—[a]	—[a]	8.02 ($n = 58$)	63.60 ($n = 3$)	159.44 ($n = 14$)

[a] Asian Dust observations (March 18–19, 2024) are confined to $T \leq -22\,°C$ because the chamber operated primarily in cold-mode expansion cycles during these events.

3.2 Temperature spectra of INP

The temperature dependence of INP concentrations differed markedly among the three datasets and across the three Jeju aerosol categories (Fig. 3 and Table 2). These spectra and corresponding bin-median statistics were derived from the PINE L2 Temp_Spec binned analysis. Arctic values represent the QC-passed, ship-contamination filtered ARAON RV dataset, while Jeju values represent day-classified processed spectra (Clean: background days, March 5, 2024; Polluted: elevated aerosol loading, March 2–3, 2024; Asian Dust: identified dust-event days, March 18–19, 2024). As reported in Table 2, values in parentheses indicate the number of valid expansion runs (n) contributing to each $\pm 0.5\,°C$ temperature bin, and dashes indicate that no valid bin observations satisfied the per-category, per-temperature criteria. At warm temperatures (-19 to $-22\,°C$), the QC-passed Arctic shipborne datasets exhibited substantially higher median concentrations than the Jeju Clean and Polluted categories: at $-19\,°C$, ARA15A 2024 reached 3.58 L^{-1} ($n = 111$) and ARA16A 2025 reached 6.75 L^{-1} ($n = 427$), compared with 0.51 L^{-1} ($n = 14$) for Jeju Clean and 1.93 L^{-1} ($n = 22$) for Jeju Polluted; at $-20\,°C$, values were 3.68 L^{-1} ($n = 173$) and 3.64 L^{-1} ($n = 593$) for the Arctic datasets versus 0.89 L^{-1} for Clean and 3.74 L^{-1} for Polluted; at $-22\,°C$, values were 3.67 L^{-1} (Arctic 2024) and 6.20 L^{-1} (Arctic 2025) versus 1.25 L^{-1} for Clean, 9.07 L^{-1} for Polluted, and 8.02 L^{-1} for Asian Dust. Below $-22\,°C$ the pattern reversed sharply for the Jeju Polluted and Asian Dust categories: at $-25\,°C$, the Jeju Polluted median (19.20 L^{-1}; $n = 22$) and Asian Dust median (63.60 L^{-1}; $n = 3$) substantially exceeded both Arctic 2024 (3.66 L^{-1}; $n = 383$) and Arctic 2025 (6.49 L^{-1}; $n = 297$), by factors of 3–10 (Polluted) and 10–17 (Asian Dust); at $-28\,°C$, the Asian Dust median reached 159.44 L^{-1} ($n = 14$), more than a factor of 20 higher than both Arctic values (7.02 and 6.39 L^{-1}), while the Jeju Polluted median (38.48 L^{-1}) remained roughly five times higher than the Arctic medians. In contrast, the Jeju Clean category remained relatively low at all temperatures (median ≤ 8.22 L^{-1} at $-28\,°C$), reflecting the absence of strong aerosol sources during background days. Asian Dust observations are confined to the cold-temperature range ($T \leq -22\,°C$) because the two qualifying dust events (March 18–19, 2024) operated the chamber primarily in cold-mode expansion cycles; this data limitation is acknowledged in the table footnotes.

https://doi.org/10.5194/egusphere-2026-3543
Preprint. Discussion started: 6 July 2026

3.3 Latitudinal distribution of INP

Figure 4 presents the latitudinal variation of INP concentrations along the full RV Araon cruise track from Incheon, Korea (≈37° N) to the high Arctic, together with the three Jeju Island event categories. The figure is divided into two regions: a *transit* section (30–65° N, covering the open-ocean passage between Korea and the Arctic) and the *Arctic observation region* (≥65° N, delineated by the dashed red box), which constitutes the primary analysis domain for the Arctic INP statistics in this study.

In the 2024 dataset (ARA15A), the highest median values along the transit were found at 30–35° N (4.06 L^{-1}; $n = 156$) and 40–45° N (3.02 L^{-1}; $n = 749$), with a pronounced minimum in the 45–55° N band (0.52–0.55 L^{-1}; $n = 149$–236). Concentrations increased again poleward within the Arctic region, with medians of 1.04 L^{-1} ($n = 196$) at 65–70° N, and 1.56 L^{-1} at both 70–75° N ($n = 473$) and 75–80° N ($n = 928$). In the 2025 dataset (ARA16A), broadly consistent transit values were observed: 1.06 L^{-1} at 40–45° N ($n = 28$), 0.53 L^{-1} at 45–50° N ($n = 112$), and 1.04 L^{-1} at 50–55° N ($n = 885$); Arctic region values were 1.00 L^{-1} at 65–70° N ($n = 707$), 1.03 L^{-1} at 70–75° N ($n = 2,107$), and 3.19 L^{-1} at 75–80° N ($n = 2,247$). The latitudinal gradient in 2024 displays a bimodal structure: elevated INP concentrations at the lowest latitudes sampled (30–40° N, likely influenced by continental aerosol outflow near Korea) and again in the high Arctic (≥75° N), separated by a mid-latitude minimum over the open North Pacific (45–60° N). Transit observations from 2025 are limited to latitudes above 40° N due to the later departure date, but confirm the mid-latitude minimum. Only data within the Arctic observation region (dashed red box, ≥65° N) are used in the inter-campaign INP comparisons reported in Sects. 3.1–3.3 and 3.5. A quantitative comparison of the PINE-derived latitudinal INP distribution at $T = -20\,°C$ with published offshore filter-based Arctic datasets is provided in Fig. S3 of the Supplement.

3.4 Ship contamination identification and removal

For the shipborne campaigns, quality control proceeded in two phases: an operation-level evaluation followed by run-level spike removal using the dual-criterion contamination test (relative wind direction within the stern sector, 135–225°, combined with INP concentration spikes exceeding ≈ 100 times the estimated clean-air background). During Arctic 2024 (ARA15A), all 4 operations passed the initial operation-level evaluation and were subjected to run-level spike removal. During Arctic 2025 (ARA16A), 19 operations were conducted. Of these, 8 operations during the inlet malfunction period (11 July – 7 August 2025) were fully excluded, including one aborted 102-second initialisation session with no data (Table S2 in the Supplement); one further operation (6–12 August 2025) fell partially within this period but yielded valid measurements from 8–12 August after the inlet was restored; and a further 4 operations with absent POPS data were excluded. The remaining 7 ARA16A operations include the 8–12 August period (991 clean runs after QC), 5 ship-exhaust-contaminated operations subjected to run-level spike removal, and 1 fully clean operation (5–6 September 2025). This yielded 7 operations contributing 11,320 L1 runs for ARA16A (Table 1), meaning 12 of the 19 operations were excluded at the operation level. The maximum INP concentration recorded during confirmed ship-spike events reached 311 L^{-1}, approximately two orders of magnitude above the 0.5–4 L^{-1} clean-period range observed during the valid operations (Fig. 5). All contamination-flagged runs were excluded from the INP concentration

https://doi.org/10.5194/egusphere-2026-3543
Preprint. Discussion started: 6 July 2026

analyses presented in Sects. 3.1–3.3 and 3.5. The dual-criterion QC scheme combining stern-sector wind exclusion with run-level spike thresholding follows the framework established by previous Arctic ship campaigns (Modini et al., 2015; Tatzelt et al., 2022); its broader applicability to future shipborne INP measurements is addressed in the Conclusions.

3.5 Comparison with parameterisations

Observed INP concentrations were compared against three temperature-resolved parameterisations overlaid on the spectra in Fig. 3a,c,e,g,i: the aerosol-concentration-dependent DeMott et al. (2010) envelope (computed for $N_{>0.5\,\mu m} = 10$–$200\ \mathrm{cm}^{-3}$), the Arctic ship-based median of Welti et al. (2020), and the classical temperature-only fit of Meyers et al. (1992). The DeMott et al. (2010) envelope — originally derived from mineral-dust-influenced measurements — systematically underestimated Arctic INP concentrations in the warm-temperature regime ($T > -22\,^{\circ}\mathrm{C}$), consistent with a contribution from non-dust (likely marine biogenic) particles not represented by the DeMott scheme. The Welti et al. (2020) curve, itself derived from open-ocean Arctic ship campaigns, traced the central tendency of the ARAON observations more closely, while the classical Meyers et al. (1992) fit lay below both ARAON datasets at warm temperatures, reflecting its mid-latitude background calibration. The biogenic-INP parameterisation of Tobo et al. (2013) was not applied here because it requires concurrent fluorescent biological aerosol particle (FBAP) number concentrations as input — typically obtained from a Wideband Integrated Bioaerosol Sensor (WIBS), which records UV-induced auto-fluorescence (~ 280 and ~ 370 nm excitation) on a single-particle basis as a proxy for primary biological aerosol — and no such instrument was deployed alongside PINE in this campaign. Qualitative inference of a biogenic contribution therefore relies on spectral shape (Sect. 2.2) rather than on parameterisation evaluation. The agreement or divergence at individual temperature bins is interpreted in the context of source attribution in Sect. 4.1, and the implications of the warm-temperature DeMott bias for future campaign design and climate-model microphysics are addressed in the Conclusions.

3.6 Sea-ice anomaly–INP statistical association

To place the ARAON observations within the longer-term context of Arctic sea-ice retreat, a multi-dataset monthly synthesis at $T = -20\,^{\circ}\mathrm{C}$ was assembled following the methodological framework described in Sect. 2.7, drawing on published Arctic campaigns for which a monthly INP time series at $T = -20\,^{\circ}\mathrm{C}$ could be reconstructed: the Filter-imm filter-based immersion-freezing assays at TROPOS-network Arctic stations (Wex et al., 2019; Hartmann et al., 2021; Sze et al., 2023), alongside the two present PINE campaigns (ARA15A 2024 and ARA16A 2025). The offline Filter-imm concentrations are harmonised to the PINE concentration scale using the $\times 11.2$ factor (Appendix A) at the $T = -20\,^{\circ}\mathrm{C}$ reference temperature, where method-specific online–offline offsets are smallest (Sect. 4.4). The DRUM cascade impactor dataset was excluded from the synthesis because its Monte Carlo PINE-to-DRUM concentration ratio at $T = -20\,^{\circ}\mathrm{C}$ is approximately 296 (Appendix A, Fig. A1b), an order of magnitude beyond the marine online–offline range documented by Wilbourn et al. (2024). The reported monthly concentrations were paired with the corresponding monthly mean Arctic SIE from the NSIDC Sea Ice Index (National Snow and Ice Data Center (NSIDC), 2024, 2025) (full campaign metadata in Supplement Table S4).

https://doi.org/10.5194/egusphere-2026-3543
Preprint. Discussion started: 6 July 2026

The synthesis comprises eight datasets totalling 56 dataset-month pairs spanning 2012–2025 (Fig. 6a). Because the raw SIE signal is dominated by the intra-annual seasonal cycle (SIE ranges from ∼4 in summer to ∼15 $\times 10^6$ km^2 in winter), the climatology was removed by subtracting the 1981–2010 monthly mean to obtain SIE anomalies (Fig. 6b). On the deseasonalised panel, a significant negative association was recovered: Spearman $\rho = -0.57$ ($p = 4.7 \times 10^{-6}$), with a Newey–West HAC-corrected OLS slope of -0.22 (95 % CI $[-0.36, -0.09]$) (Newey and West, 1987); residual autocorrelation diagnostics are reported in Supplement Table S7. Restricted to the Filter-imm subset (PINE excluded; $n = 52$ months), the association remains significant: Spearman $\rho = -0.53$ ($p = 5 \times 10^{-5}$), HAC-corrected OLS slope -0.17 (95 % CI $[-0.28, -0.06]$; Supplement Table S7).

Sensitivity of the regression to the Filter-imm harmonisation factor (from $\times 1$, CF-naive, to $\times 47$) is documented in Supplement Fig. S7, where the rank-order (Spearman) association remains robust ($\rho = -0.46$ to -0.58). Concurrent daily satellite observations during August–September 2024 yielded a negative association between Arctic SIE and surface chlorophyll-a concentration in the central Arctic Ocean (Pearson $r = -0.52$, $p < 0.001$, $n = 55$; Fig. 6c). Interpretation of the SIE–INP association — including method/SIE confounding, alternative drivers, and causal hypothesis evaluation — is deferred to Sect. 4.5.

4 Discussion

4.1 Source characteristics inferred from INP temperature spectra

All source interpretations in the present discussion are inferential, based on spectral-shape consistency with literature parameterisations for known source types rather than direct heat-treatment experiments or aerosol chemical composition measurements, neither of which were performed in this study; they should be read as "consistent with" rather than as direct demonstrations of source identity. With this caveat in mind, the contrasting shapes of the INP temperature spectra observed at high Arctic latitudes and at Jeju Island are consistent with different prevailing INP source contributions at each location. In the Arctic, elevated INP concentrations were observed predominantly in the warm temperature regime, consistent with a marine biogenic-influenced regime in which sea-surface microgels, ice-melt-associated organic matter, and exudates from phytoplankton blooms have been proposed as plausible contributors (Bigg and Leck, 2001; Creamean et al., 2018; Irish et al., 2019; DeMott et al., 2016; McCluskey et al., 2018; Porter et al., 2022; Ickes et al., 2020; Wilbourn et al., 2020). In contrast, the Jeju INP spectra were characterised by a steep increase in concentration at temperatures below $-22\,^\circ$C, consistent with the spectral signature of mineral dust particles, including Asian dust transported across the mid-latitude westerly belt (Murray et al., 2012; Atkinson et al., 2013; Chen et al., 2018; Tobo et al., 2019; Price et al., 2018). The spectral crossover — where Arctic INP concentrations exceed Jeju values at warm temperatures but fall below at cold temperatures — is consistent with contrasting rather than mutually exclusive source contributions, in line with the marine biological INP parameterisation proposed by Wilson et al. (2015).

A further feature consistent with this contrasting-source interpretation is the anomalously weak temperature dependence of the Arctic spectra. The ARAON datasets exhibit a markedly flat slope ($\beta = \mathrm{d}\log_{10}(\mathrm{INP})/\mathrm{d}T \approx -0.022\,\mathrm{K}^{-1}$, ∼1.7-fold per $10\,^\circ$C cooling), whereas single-location Arctic datasets typically cluster around $\beta = -0.07$ to $-0.09\,\mathrm{K}^{-1}$ (Sect. 4.4). Several

https://doi.org/10.5194/egusphere-2026-3543
Preprint. Discussion started: 6 July 2026

lines of evidence indicate that this flatness is an intrinsic characteristic of the sampled marine Arctic boundary layer rather than an artefact of aggregating sources along the cruise track. First, the flat slope persists within individual operations, including segments spanning less than half a degree of latitude over a few hours that sample an approximately single air and water mass (per-operation slope breakdown, Fig. S8 in the Supplement); narrowing the spatial window therefore does not recover the steep single-location slope that along-track mixing of populations with differing onset temperatures would produce. Second, the same PINE instrument family deployed at the continental, sub-Arctic Sammaltunturi site (PaCE-2022) returns the steep $\beta = -0.07$ to $-0.09\,\mathrm{K}^{-1}$ typical of single-location records (Böhmländer et al., 2025), indicating that the flat ARAON slope reflects the marine Arctic regime rather than a universal PINE behaviour. Third, comparably shallow open-ocean spectra have been reported from ship-based Arctic surveys (Welti et al., 2020). The persistently elevated warm-temperature end (-15 to $-22\,^{\circ}\mathrm{C}$) responsible for the flatness is consistent with a contribution from heat-labile marine-biogenic INP — identified as the dominant warm-temperature INP type in summer Arctic marine air by the offline filter studies of Porter et al. (2022) and Creamean et al. (2022) — set against the low background concentrations and large spatial variability documented for the remote Arctic Ocean by Li et al. (2025).

A marine-specific measurement effect plausibly reinforces this intrinsic flatness. The temperature-dependent online–offline offset documented for PINE in marine air (Wilbourn et al., 2024) acts in the same sense, raising PINE-measured concentrations preferentially at the warm-temperature end (Sect. 4.4); being marine-specific, it would flatten the ARAON spectra while leaving the continental PaCE-2022 slope steep, consistent with the instrument contrast noted above. The value $\beta \approx -0.022\,\mathrm{K}^{-1}$ should accordingly be read as a property of the marine Arctic regime as sampled by an online expansion chamber, not as a quantity directly comparable to slopes from offline filter assays. Disentangling the biogenic, mineral, and instrumental contributions to the warm-temperature signal awaits the heat-treatment and composition measurements discussed below.

Three alternative mechanisms for the warm-temperature Arctic enhancement cannot be excluded on spectral evidence alone. First, long-range transport of ice-nucleating mineral dust from high-latitude glaciogenic and periglacial sources — including Svalbard outwash plains, Greenlandic glacial valleys, and expanding periglacial terrain under permafrost thaw (Kawai et al., 2023; Sanchez-Marroquin et al., 2020) — could contribute to warm-temperature INP without a biological mechanism. Second, sea-spray-associated inorganic INP, including iron-bearing particles and organically-coated sea-spray, can activate at temperatures above $-20\,^{\circ}\mathrm{C}$ (Wilbourn et al., 2020) and would be indistinguishable from biogenic material on spectral grounds without heat-treatment. Third, the elevated INP concentrations in ARA16A relative to ARA15A at the 75–80° N band (Sect. 3.3) may reflect interannual variability in large-scale atmospheric circulation (e.g., Arctic Oscillation index differences) rather than a change in biogenic source strength. Resolution of these competing hypotheses requires future campaigns combining parallel heat-treated sampling (95°C for 20 min), inductively coupled plasma mass spectrometry (ICP-MS) or X-ray fluorescence for mineral tracers (Al, Fe, Ti), and fluorescence spectroscopy or flow cytometry for biological particle identification (Bigg and Leck, 2001; DeMott et al., 2016).

https://doi.org/10.5194/egusphere-2026-3543
Preprint. Discussion started: 6 July 2026

4.2 Latitudinal variation and potential source regions

The latitudinal distribution of INP concentrations along the cruise track revealed a non-monotonic pattern that is difficult to reconcile with a single dominant source region. In the 30–45° N latitude band, median INP concentrations of 2.6–4.1 L^{-1} likely reflect a mixed signal from continental aerosol outflow originating over the Yellow Sea and East China Sea, where Asian dust and anthropogenic aerosols are frequently advected offshore by prevailing westerlies (Uno et al., 2009). In the 45–55° N range, a relative minimum (Sect. 3.3) is consistent with sampling of cleaner North Pacific or Bering Sea maritime air masses with reduced continental aerosol loading. The re-emergence of elevated INP concentrations at 75–80° N (median 1.56 L^{-1} in 2024 and 3.19 L^{-1} in 2025) is potentially associated with enhanced biogenic activity near the marginal ice zone (MIZ), where sea-ice melt and phytoplankton blooms are known to supply organic material to the marine boundary layer (Creamean et al., 2018; Zeppenfeld et al., 2019; Gong et al., 2020; Ickes et al., 2020). The overall weak latitudinal gradient suggests that INP concentrations along this transect were governed more by source characteristics at each latitude than by a simple meridional transport gradient.

The sign of the interannual contrast is reversed between low and high latitudes: at 40–45° N (mid-Pacific transit), ARA15A 2024 concentrations (3.02 L^{-1}; $n = 749$) substantially exceeded those of ARA16A 2025 (1.06 L^{-1}; $n = 28$), whereas at 75–80° N the 2025 median was approximately twice that of 2024. This decoupling suggests that interannual variability in Asian continental outflow is independent of variability in Arctic biogenic activity. Although campaign-wide medians (ARA15A: 6.83 L^{-1}; ARA16A: 6.57 L^{-1}) appear broadly comparable, this aggregation masks the latitude-resolved interannual signal, which may partly reflect interannual variability in large-scale circulation patterns such as the Arctic Oscillation or variations in sea-ice extent. A more definitive attribution would require concurrent trajectory analysis and marine biogeochemical measurements.

4.3 Uncertainties and limitations

Several sources of uncertainty must be acknowledged when interpreting the present results. The INP concentration measurements carry a combined uncertainty comprising a Type A (random) component estimated from Poisson counting statistics and a Type B (systematic) component of approximately 10%, introduced by uncertainties in the sampled air volume and the impinger collection efficiency of the PINE instrument. Additionally, the PINE gas-phase temperature sensor may carry a systematic offset (ΔT) of up to 1.0 K relative to the actual droplet temperature during adiabatic expansion (Möhler et al., 2021); propagating this worst-case offset through the campaign-specific temperature sensitivities (β; Sect. 2.6) yields maximum INP changes of $\approx 5\,\%$ for the Arctic campaigns and $\approx 17\,\%$ for Jeju. No explicit ΔT correction was applied: the Arctic impact ($\approx 5\,\%$) is smaller than the CF uncertainty, whereas the Jeju impact ($\approx 17\,\%$) does not alter the sign of inter-campaign comparisons but should be borne in mind for absolute values (Fig. S1 in the Supplement). The measurement durations and operational statistics for the three field deployments are summarised in Table 1. Over the entire study period, a total of 41,524 expansion runs were performed, with 35,370 runs successfully passing standard QC and ship-contamination filters (Sect. 2.5.2). The 2024 Arctic campaign (ARA15A) included only four valid operational sampling periods after QC, reducing the statistical robustness of derived medians. Furthermore, heat treatment experiments — a standard method for distinguishing heat-labile biogenic INPs

https://doi.org/10.5194/egusphere-2026-3543
Preprint. Discussion started: 6 July 2026

from heat-stable mineral dust INPs — were not performed during either campaign, precluding direct quantification of the biogenic INP fraction. Future campaigns should prioritise parallel heat-treatment experiments and continuous aerosol chemical composition measurements to enable more definitive source apportionment.

Four potential sampling biases are assessed here. (i) **Inlet height**: the PINE inlet was located at ∼10 m a.s.l. on ARA15A and ∼7 m on ARA16A. Both heights sample within the marine surface boundary layer; the 3 m difference is estimated to introduce $< 5\,\%$ change in coarse-mode sea-spray concentration and $< 7\,\%$ in INP via the DeMott et al. (2010) parameterisation. No height correction was applied. (ii) **Diurnal bias**: PINE operated continuously throughout each operation. A Kruskal–Wallis test across four time-of-day quartiles (00–06, 06–12, 12–18, 18–24 UTC) for ARA16A 2025 yielded $H = 8.59$, $p = 0.035$; however, the quartile medians spanned only 6.51–6.60 L^{-1} (range $< 2\,\%$), indicating the statistical significance arises from the large sample size ($n_{\mathrm{per\ quartile}} \approx 1,400$) rather than a practically meaningful diurnal signal. This interpretation is consistent with the expectation of minimal diurnal aerosol cycling under the 24-hour polar-day conditions of the summer Arctic. (iii) **Sea state**: wave-enhanced sea-spray production during high sea states could transiently elevate INP. Analysis of ship motion records for ARA16A indicated no correlation between significant wave height proxies and INP concentration on the operation timescale. (iv) **Calibration drift**: PINE was calibrated at the Bilfinger Noell facility before each campaign using NIST-traceable references; pre- and post-campaign blank expansions confirmed < 0.2 background ice events per expansion, and the consistency of clean-period medians between ARA15A and ARA16A (6.83 vs 6.57 L^{-1}) suggests inter-campaign calibration drift $< 5\,\%$.

A related point concerns the appropriate counting unit for statistical degrees of freedom. The total of 41,524 PINE expansion runs — 11,854 (ARA15A), 11,320 (ARA16A), and 18,350 (Jeju 2024) — counts individual cycle measurements; for between-condition inference, however, runs within the same operation, hour, day, or air mass are not statistically independent because they sample broadly the same meteorological and source conditions. Effective independent sample counts at progressively coarser aggregation scales are reported in Supplement Table S8 and are summarised here as a hierarchy: the run count overstates statistical degrees of freedom by approximately one to three orders of magnitude relative to the operation-level count (4 for ARA15A, 7 for ARA16A, 20 for Jeju 2024), and by an intermediate factor relative to the air-mass-distinct sampling segments along the cruise track (estimated at ∼30–40 segments per Arctic campaign on a 1-degree latitude binning, equivalent to ∼25–35 distinct sampling days). Per-temperature-bin medians cited in the present study (e.g., $n = 8$ at $T = -22\,^{\circ}\mathrm{C}$ for ARA15A) report the number of QC-passed runs reaching that specific temperature bin, not an underlying independent-sample n; their interpretation as cluster-level summaries is preserved by the source–regime contrasts being reported as differences between campaign-level central tendencies (Sect. 2.2, Sect. 3.2) rather than as n-dependent significance tests at each temperature bin.

The robustness of the ship-contamination QC scheme to the specific numerical thresholds chosen in Sect. 2.5.2 (criteria 1–4) was evaluated by perturbing each threshold by $\pm 50\,\%$ and re-running the full QC pipeline; campaign-median INP concentrations at $T = -20\,^{\circ}\mathrm{C}$ and $-25\,^{\circ}\mathrm{C}$ and the inter-campaign rank ordering were preserved under all threshold combinations tested, with $< 5\,\%$ change in any reported median (full breakdown in Supplement Table S3). We note, however, that this sensitivity analysis was conducted on campaign-median statistics; threshold choices may have larger impacts on extreme percentiles or specific warm-regime sub-populations, which warrants further investigation. The fixed CF $= 16$ used for cross-method compar-

https://doi.org/10.5194/egusphere-2026-3543
Preprint. Discussion started: 6 July 2026

ison is similarly framed only as a first-order, order-of-magnitude working approximation valid near the $T = -20\,^{\circ}\mathrm{C}$ reference temperature (Sect. 4.4, Appendix A); it is not a calibration transfer and is not applied to temperature-resolved slope derivation or to absolute-rate trend attribution. The single-temperature regression reported in Sect. 3.6 is interpreted as a descriptive association measure evaluated at the $T = -20\,^{\circ}\mathrm{C}$ reference point, not as a calibrated rate.

4.4 Inter-method comparison: PINE versus offline-filter INP concentrations

Figure 7 presents an integrated comparison of INP concentration spectra from the Arctic ARAON campaigns, the Jeju K-CPEC site, the PaCE-2022 sub-Arctic observations, and the Wilbourn et al. (2024) ENA online–offline pair. The overlaid ENA pair (PINE-03 online vs. WT-CRAFT offline) makes the regime-dependent online–offline offset directly visible: the two curves diverge from a factor of ∼3 at $T = -25\,^{\circ}\mathrm{C}$ to ∼80 at $T = -15\,^{\circ}\mathrm{C}$, a temperature-dependent marine offset that increases towards warmer temperatures. This integrated view frames the central methodological question of this section — how to place online expansion-chamber (PINE) and offline filter-based INP measurements on a common, quantitatively defensible scale — and both motivates and brackets the fixed harmonisation factor (CF = 16) derived in the remainder of this subsection.

A rigorous comparison between online expansion-chamber instruments such as PINE and the offline filter-based assays that underpin most of the historical Arctic INP record requires placing the two on a common scale. The entire inter-method comparison in this study is conducted in INP number concentration space (L^{-1}). For first-order, order-of-magnitude harmonisation near the $T = -20\,^{\circ}\mathrm{C}$ reference temperature we adopt a single fixed correction factor, CF = 16, computed as the median ratio of the PINE $T = -20\,^{\circ}\mathrm{C}$ concentration distribution to a pooled Filter IS distribution (Wex et al., 2019; Hartmann et al., 2021; Barry, 2024), with a 95 % uncertainty range of 8–28 obtained from Monte Carlo propagation of run-level variability (full derivation, including the complementary median-ratio estimate and its temperature dependence, in Appendix A). Because the PINE and Filter IS distributions used in this derivation are not co-located in space, season, or aerosol regime, CF = 16 is an empirically motivated harmonisation factor rather than a calibration transfer; three lines of published evidence support this value as a physically reasonable first-order approximation for Arctic marine boundary-layer conditions.

First, the PINE chamber samples a broader size and freezing-mode population than immersion-only offline filter assays — pore-condensation freezing and deposition freezing modes contribute to PINE activation at warm temperatures but are typically not accessed by water-suspended offline protocols (Möhler et al., 2021) — providing a physical basis for systematic PINE/filter concentration offsets. Second, the Puy de Dôme Ice Nucleation Intercomparison Campaign (PICNIC) at the Puy de Dôme high-altitude observatory compared 10 INP methods (3 online, 7 offline) in continental, dust-influenced aerosol and found that the majority of measurements agreed within a factor of ∼5, with PINE in particular agreeing with the Colorado State University Continuous Flow Diffusion Chamber (CSU-CFDC) reference within a factor of ∼2 for 71 % of the data (Lacher et al., 2024; DeMott et al., 2018), setting a lower bound on the online–offline offset in regimes dominated by mineral-like activation. Third, and most directly relevant to the marine Arctic regime sampled here, Wilbourn et al. (2024) simultaneously co-deployed the online PINE-03 chamber and offline immersion-freezing assays at two U.S. Department of Energy Atmospheric Radiation Measurement (ARM) observatories: the continental Southern Great Plains (SGP) site, paired with the Ice Nucleation Spectrometer of the Karlsruhe Institute of Technology (INSEKT) filter assay, and the remote-marine Eastern North

https://doi.org/10.5194/egusphere-2026-3543
Preprint. Discussion started: 6 July 2026

Atlantic (ENA) site in the Azores, paired with the West Texas Cryogenic Refrigerator Applied to Freezing Test (WT-CRAFT) filter assay. At SGP the online and offline N_{INP} medians at $T = -20\,^{\circ}\mathrm{C}$ agreed closely ($\sim 2\ \mathrm{L}^{-1}$ for both), whereas at ENA the online PINE-03 exceeded the offline WT-CRAFT by 1–2 orders of magnitude — a marine-specific offset that Wilbourn et al. (2024) attributed primarily to filter sampling inefficiencies, with possible additional contributions from chemical denaturation of marine-biogenic INPs (Wilson et al., 2015; McCluskey et al., 2018).

CF = 16 (uncertainty 8–28) therefore sits between the continental ∼5 agreement bound of Lacher et al. (2024) and the marine 10–100 discrepancy reported by Wilbourn et al. (2024), quantitatively consistent with the published range of PINE-vs-filter offsets for Arctic marine boundary-layer conditions. The regime- and temperature-dependence is critical: a fixed CF is appropriate only for order-of-magnitude harmonisation near the $T = -20\,^{\circ}\mathrm{C}$ reference point, never for temperature-resolved slope derivation or absolute-rate trend attribution. Applying CF = 16 to the PINE Arctic data yields approximate agreement with the seasonal envelope of historical Arctic observations (within 0.05–0.5 L^{-1}; Fig. S2 and Fig. S4 in the Supplement); a dedicated comparison with the sub-Arctic Pallas Cloud Experiment 2022 (PaCE-2022) PINE deployment at Sammaltunturi (Böhmländer et al., 2025) is shown in Fig. S5.

Beyond motivating the harmonisation factor, the temperature dependence of this offset carries a geophysical implication for the warm-temperature regime. That the ENA online–offline divergence grows to ∼80-fold by $T = -15\,^{\circ}\mathrm{C}$ (Wilbourn et al., 2024), and that the ARAON warm-temperature (-15 to $-20\,^{\circ}\mathrm{C}$) concentrations sit well above the offline-filter Arctic Ocean record (Sect. 4.1), together indicate that much of the warm-active marine INP population is not retained by integrated offline assays. Warm-temperature marine INP are predominantly heat-labile biological particles (Porter et al., 2022; Creamean et al., 2022) that are sporadic in time and vulnerable to loss through filter collection inefficiency, multi-hour integration, and freeze–thaw denaturation during storage; a continuous online chamber that samples large air volumes without substrate storage is intrinsically better suited to capturing them. Because every prior shipborne Arctic Ocean INP dataset relies on offline filter assays — or, for the cold-temperature range only, on continuous-flow diffusion chambers (Porter et al., 2022; Creamean et al., 2022; Li et al., 2025) — real-time PINE provides a more faithful, continuous depiction of warm-temperature marine ice-nucleating activity, the regime most relevant to Arctic mixed-phase clouds, than has previously been available over the open Arctic Ocean. We frame this as an advantage specific to the warm-temperature biological population rather than a claim of absolute accuracy: the expansion chamber additionally accesses pore-condensation and deposition freezing modes whose cloud relevance is mode-dependent, so the inter-method comparison remains order-of-magnitude and the fixed CF is retained only to place PINE on the established filter scale, not to designate either method as the reference truth.

Temperature dependence ($\beta = \mathrm{d}\log_{10}(\mathrm{INP})/\mathrm{d}T$) provides a complementary diagnostic. Single-location Arctic datasets — PaCE-2022 (Böhmländer et al., 2025), the Multidisciplinary drifting Observatory for the Study of Arctic Climate (MOSAiC; Creamean et al. 2022), and the Filter IS and DRoplet Ice Nuclei Counter Zurich (DRINCZ) datasets of Barry (2024); Li et al. (2025) — cluster around $\beta = -0.07$ to -0.09 (a 7–9-fold INP increase per 10 °C cooling), whereas the ARAON datasets exhibit a markedly flatter slope ($\beta \approx -0.022\,\mathrm{K}^{-1}$, ∼1.7-fold per 10 °C; per-campaign regression statistics in Sect. 2.6 and Table S6 in the Supplement). As developed in Sect. 4.1, this flatness appears intrinsic to the sampled marine Arctic boundary layer rather than a product of along-track source mixing: the flat slope persists within individual operations, and the same

https://doi.org/10.5194/egusphere-2026-3543
Preprint. Discussion started: 6 July 2026

instrument at the continental PaCE-2022 site (Böhmländer et al., 2025) returns the steep $\beta = -0.07$ to -0.09 of single-location records, with the marine-specific temperature-dependent online–offline offset (Wilbourn et al., 2024) reinforcing the flattening. A preliminary long-term assessment spanning 2019–2025 tentatively suggests an increase in method-corrected Arctic summer INP coinciding with record-low Arctic sea-ice extent in the 2024–2025 summer seasons reported by the National Snow and Ice Data Center (National Snow and Ice Data Center (NSIDC), 2025); given the limited number of independent years ($n = 5$) and substantial CF uncertainties, this apparent trend should be regarded as a hypothesis for future targeted, co-located multi-instrument campaigns.

4.5 Interpretation of the sea-ice/INP association

The deseasonalised SIE–INP association reported in Sect. 3.6 quantifies an observational *association*, not a causal relationship. The present analysis cannot, on its own, demonstrate that sea-ice loss drives INP enhancement, because (i) method and SIE are partially confounded across the multi-dataset record (the two PINE campaigns are also the two lowest-SIE years), (ii) no direct chemical or biological speciation of the high-INP particles was performed, and (iii) plausible alternative drivers — including independent variability in atmospheric circulation patterns, expanded periglacial dust sources (Kawai et al., 2023), and decadal trends in marine biogeochemistry — could co-vary with sea-ice extent without implying causation. With these caveats stated explicitly, the present synthesis is intended only as an empirical pattern that motivates future co-located, multi-instrument process studies; it should not be cited as direct evidence of a sea-ice-driven biogenic-INP mechanism.

A critical caveat concerns method–SIE confounding. The multi-dataset monthly synthesis aggregates two main measurement techniques (Filter-imm and PINE); notably, the two PINE campaigns are also the two most recent years with the lowest SIE values. A possible contributing factor is that historical filter-based (offline) methods can dilute transient, high-concentration INP events over long integration times (24–72 hours), and may underestimate fragile marine biological INPs through sample storage, freeze–thaw cycles, and background filter contamination, whereas the online PINE chamber performs rapid adiabatic expansions that avoid substrate degradation. Whether these instrument-specific differences contribute materially to the apparent SIE/INP signal — versus residual inter-instrument bias not absorbed by the harmonisation factors of Table A1 — cannot be resolved with the present dataset. The persistence of the negative association in the PINE-excluded Filter-imm-only subset (Sect. 3.6) is the most direct quantitative response to this concern: the SIE anomaly–INP relationship is not an artefact of the two PINE campaigns alone. Nevertheless, direct testing of the underlying mechanism requires co-located online and offline instrumentation operated through a contiguous low-SIE / high-SIE record.

This preliminary association is consistent with a growing body of literature pointing to a coupled biological-cryospheric emission mechanism. For instance, year-round observations in the central Arctic by Creamean et al. (2022) demonstrate a distinct annual cycle where INP concentrations peak during the summer melt season, driven by local marine biological production in newly exposed open waters. Similarly, Wex et al. (2019) and Hartmann et al. (2021) observed elevated biogenic INP signatures during Arctic summer melt periods. The concurrent satellite SIE–chlorophyll-a association documented in Sect. 3.6 (Fig. 6, panel c) provides a basin-scale observational context: as proposed by prior studies (Wilson et al., 2015; Irish et al., 2019; Willis et al., 2018), increased primary productivity in expanded open-water areas enriches the sea surface microlayer with

https://doi.org/10.5194/egusphere-2026-3543
Preprint. Discussion started: 6 July 2026

marine organic exudates that may act as efficient INPs. The ARAON datasets, representing the most recent years of advanced sea-ice retreat, exhibit the highest measured INP concentrations within our multi-dataset synthesis. This observational pattern is consistent with the hypothesis that reduced sea-ice cover may be associated with enhanced biogenic INP emissions, though the causal mechanisms remain to be confirmed through targeted, co-located multi-instrument campaigns. This hypothesis is not mutually exclusive with the model-based attribution of Kawai et al. (2023), which identified Arctic dust as the dominant summertime INP source in a large-scale aerosol simulation: both source types (mineral dust from newly exposed periglacial surfaces, and marine organics from productive open water) are expected to increase under advanced sea-ice retreat, so the direction of the SIE/INP relationship is plausibly consistent under either attribution. Our observations cannot arbitrate between the two on spectral grounds alone, and we interpret the Kawai result as complementary motivation for co-located chemical composition measurements in future campaigns rather than as evidence against the marine-biogenic pathway.

5 Conclusions

This study presents the first systematic multi-year PINE-based characterisation of INP concentrations across complementary Arctic shipborne (RV Araon ARA15A 2024, ARA16A 2025) and East Asian continental-outflow (K-CPEC, Jeju Island, 2024) environments. As the first online expansion-chamber INP deployment over the Arctic Ocean, these campaigns show that continuous, high-volume real-time sampling captures the warm-temperature, heat-labile marine-biogenic INP that integrated offline-filter assays tend to underestimate, making real-time shipborne measurement particularly well suited to characterising warm-temperature marine ice-nucleating activity. The contrasting spectral shapes between sites — warm-temperature enhancement in the Arctic and cold-temperature steepening at Jeju — are consistent with different prevailing source regimes (marine biogenic and Asian dust, respectively), and the bimodal latitudinal structure observed along the RV Araon transect (mid-latitude continental outflow and Arctic marginal-ice-zone enhancement, separated by a clean North Pacific minimum) further underscores the multi-source character of the sampled marine boundary layer. Resolving the relative contributions of marine biogenic emissions and high-latitude periglacial dust to the warm-temperature Arctic signal must await co-deployed compositional measurements (heat-treatment, ICP-MS, fluorescence speciation) and remains an open research priority.

A central observational result is the significant negative association between Arctic INP concentrations and deseasonalised sea-ice extent anomalies in our multi-dataset monthly synthesis, robust to PINE-exclusion and to Newey–West HAC-corrected inference. Read together with the concurrent satellite SIE–chlorophyll-a coupling, this pattern is consistent with — but does not by itself diagnose — the hypothesis that retreating Arctic sea-ice enhances marine biogenic INP emissions through expanded open-water primary productivity. Whether method/year confounding or genuine biogeochemical drivers underlie this signal cannot be resolved with the present dataset; targeted co-located online–offline campaigns spanning a contiguous low/high-SIE record will be required to test the proposed coupling mechanism.

The systematic warm-temperature underestimation by the DeMott et al. (2010) parameterisation reinforces ongoing calls for ocean-specific INP parameterisations that explicitly account for marine biogenic sources (Wilson et al., 2015; Vergara-Temprado et al., 2017, 2018). Mineral-dust-centric INP schemes employed in atmospheric models including the Weather

https://doi.org/10.5194/egusphere-2026-3543
Preprint. Discussion started: 6 July 2026

Research and Forecasting model (WRF) and the NCAR Community Atmosphere Model version 6 (CAM6) are likely to misrepresent mixed-phase cloud glaciation in remote marine and polar regions where biogenic INP contributions are thought to be substantial (Tan et al., 2016; Shi and Liu, 2019), with attendant consequences for simulated cloud-phase feedbacks and climate sensitivity. The combined ARA15A/ARA16A and K-CPEC dataset provides observational benchmarks at $T = -20$ to $-25\,^{\circ}\mathrm{C}$ suitable for evaluating these parameterisations in model frameworks such as CAM6 and EC-Earth.

The methodological framework introduced here — a two-phase shipborne quality control scheme combining stern-sector wind exclusion with run-level spike thresholding, and a literature-justified order-of-magnitude correction factor (CF = 16) for placing online expansion-chamber data on the historical offline-filter scale — provides a replicable foundation for future shipborne INP campaigns. The fixed correction factor is regime- and temperature-dependent and serves only for first-order harmonisation at the $T = -20\,^{\circ}\mathrm{C}$ reference point; a temperature- and composition-resolved inter-method transfer will require co-located, simultaneous PINE and offline-filter deployment across marine-biogenic and continental/dust regimes. Future ARAON-class deployments equipped with WIBS or comparable fluorescent bioaerosol instrumentation co-located with the PINE inlet, complemented by parallel heat-treatment INP sampling and bulk aerosol chemical speciation, will be necessary to quantitatively test biogenic-INP parameterisations against shipborne datasets and to arbitrate marine-biogenic versus mineral-dust contributions to warm-temperature Arctic INP. Because the warm-temperature marine INP population is dominated by fragile biological particles prone to offline sampling and storage losses, the real-time online expansion-chamber approach deployed here offers a complementary and, for that regime, more faithful observational window than the offline-filter methods underpinning the historical Arctic Ocean record — an advantage specific to warm-temperature marine ice-nucleating activity rather than a claim of absolute accuracy.

Code and data availability. The Level-1 (run-level) and Level-2 (temperature-binned) ice-nucleating particle (INP) concentration products for the RV Araon Arctic campaigns (ARA15A, 2024; ARA16A, 2025) and the Jeju 2024 campaign, the PaCE-2022 PINE data, the quality-control tables, all derived data files underlying the figures and tables, and the complete Python analysis code (quality control, ship-contamination removal, Monte Carlo correction-factor propagation, and figure/table generation) are openly available on Zenodo under the Creative Commons Attribution 4.0 International (CC-BY-4.0) licence (DOI: `10.5281/zenodo.20724286`). The post-processing code that derives the Level-1/Level-2 products from the PINE Analysis software (PIA v3.1.0) output is included; PIA itself is the proprietary PINE instrument-analysis software of the Karlsruhe Institute of Technology (KIT) and is not redistributed here. During peer review the archive is accessible to referees and editors through a restricted-access Zenodo reviewer link registered in the Copernicus assets system. The third-party Wilbourn et al. (2024) PINE-03 and offline-filter (INSEKT, WT-CRAFT) datasets used for the ENA online–offline overlay in Fig. 7 and Fig. S6 were obtained from the PANGAEA repository (Wilbourn and Hiranuma 2023; DOI 10.1594/PANGAEA.964038, licence CC-BY-4.0). The final Zenodo DOI will replace the placeholder identifier in the accepted version.

Author contributions. JWC: Conceptualization, Data curation, Formal analysis, Investigation, Methodology, Visualization, Writing – original draft, Writing – review & editing. BYK, MB, YSO, MK, and SK: Data curation, Investigation (observation data processing and operation). YJY, JYP, and SJP: Resources, Investigation (ARAON RV operation, KOPRI logistics and platform support). All authors reviewed and approved the final manuscript.

https://doi.org/10.5194/egusphere-2026-3543
Preprint. Discussion started: 6 July 2026

Competing interests. The contact author has declared that none of the authors has any competing interests.

Acknowledgements. We express our sincere gratitude to the captain and crew of the RV Araon for their exceptional support during the ARA15A and ARA16A Arctic expeditions.

Financial support. This research was supported by the Korea Meteorological Administration Research and Development Program "Research on Weather Modification and Cloud Physics" under Grant (KMA2018-00224) and the Korea Polar Research Institute (KOPRI) project PE2601 .

Appendix A: Correction factor details

Method-specific multiplicative Correction Factors (CF) are tabulated here for the various published INP datasets relevant to the multi-dataset sea-ice synthesis (Sect. 3.6), characterising the order-of-magnitude harmonisation framework on a common PINE-equivalent concentration scale at the $T = -20\,^{\circ}\mathrm{C}$ reference temperature (Table A1). The Filter-imm factor ($\times 11.2$) is applied to the offline subset in the regression of Sect. 3.6 to place the online (PINE) and offline data on a common concentration scale at the single reference temperature where method offsets are smallest; the remaining tabulated factors (Filter IS, DRINCZ) are reference values for datasets that do not enter the synthesis. The full sensitivity of the sea-ice regression to the Filter-imm factor (from $\times 1$, CF-naive, to $\times 47$) is documented in Supplement Fig. S7. All factors operate purely in INP number concentration space.

The PINE-vs-Filter IS concentration ratio used here as the principal reference offset, $\mathrm{CF}_{\mathrm{PINE}\rightarrow\mathrm{Filter}} \approx 16$ (95 % range 8–28; Sect. 4.4), was estimated as an order-of-magnitude harmonisation factor rather than a formally calibrated transfer standard. While it was constrained by Monte Carlo propagation of typical run-level distributional offsets ($N = 100{,}000$ realisations) at $T = -20\,^{\circ}\mathrm{C}$, we caution that applying a single fixed factor cannot fully capture the dynamic complexity of online–offline offsets.

A0.1 Monte Carlo methodology.

The Monte Carlo propagation of PINE/Filter IS ratio uncertainty used in Figs. A1b,c and A2 assumes independent log-normal sampling of (i) the PINE temperature-bin INP concentration distribution, with $\mu_{\mathrm{PINE}} = \log(\mathrm{median})$ and $\sigma_{\mathrm{PINE}} = \frac{1}{2}\log(p_{84}/p_{16})$ estimated from the empirical 16th/84th run-level percentiles within each $1\,^{\circ}\mathrm{C}$ bin (Sect. 2.6); and (ii) the Filter IS reference distribution anchored to the Barry (2024) MOSAiC corrected-concentration median at $T = -20\,^{\circ}\mathrm{C}$, with σ_{Filter} derived from the published 16th/84th CF percentiles and the temperature-scaling exponent $\beta_{\mathrm{ref}} = -0.087$ (Wex et al. 2019 Arctic annual mean). The PINE and Filter IS draws are independent, and the ratio distribution is constructed sample-wise as $r_i = N_{\mathrm{INP,PINE},i}/N_{\mathrm{INP,Filter},i}$ with $N = 100{,}000$ realisations per temperature bin under fixed random seed for reproducibility. Below-LOD censoring follows the Poisson 3-crystal threshold ($N_{\mathrm{INP}} < 3.0/V_{\mathrm{expansion}}$, $V_{\mathrm{expansion}} = 1.81$ stdL; Sect. 2.6); censored runs are excluded prior to bin-statistic computation rather than imputed. The full sampling code and intermediate distributions are provided in the data archive cited under "Data availability".

https://doi.org/10.5194/egusphere-2026-3543
Preprint. Discussion started: 6 July 2026

The non-PINE methods are listed in Table A1. The TROPOS filter-based immersion-freezing droplet-assay dataset (Filter-imm; Wex et al. 2019; Hartmann et al. 2021; Sze et al. 2023) is the only offline method actually applied in the present Fig. 6 synthesis because it provides continuous, long-term weekly/monthly measurements spanning several years, ensuring statistical representativeness when paired with monthly mean NSIDC Sea Ice Extent anomalies. The remaining datasets are tabulated for methodology-framework completeness but are not used in the monthly synthesis for the following specific methodological and physical reasons:

1. **Filter IS (Barry, 2024) and DRINCZ (Li et al., 2025)**: While their PINE-scale median scaling factors are well defined ($\times 7$ and $\times 61$ respectively; Table A1), they represent short-term, episodic campaigns. Utilizing their limited sampling days to represent a full "monthly mean" INP concentration would introduce substantial representativeness errors and statistical biases when paired with climatological sea-ice indices.

2. **CSU Ice Spectrometer (Creamean et al., 2022)**: These measurements were collected during a highly specific central pack ice drift regime which represents a geographically and physically distinct boundary layer environment compared to the coastal and marginal-ice-zone (MIZ) marine boundary layer environments of PINE and TROPOS, preventing seamless integration.

3. **DRUM (Creamean et al., 2022)**: Excluded because the Monte Carlo PINE-to-DRUM concentration ratio at $T = -20\,^{\circ}\mathrm{C}$ is approximately 296 (Fig. A1b), an order-of-magnitude offset that exceeds the marine online–offline range documented by Wilbourn et al. (2024) and falls outside the harmonisation framework that brackets the other datasets. A dedicated co-located inter-calibration would be required before inclusion.

The Filter-imm $\times 11.2$ and PINE $\times 1$ factors place the published offline and online INP records on a common (PINE) concentration scale near the $T = -20\,^{\circ}\mathrm{C}$ reference point and are applied to the Filter-imm subset in the regression of Sect. 3.6. Because a harmonisation factor is applied to one subset (offline) while the other is held at $\times 1$ (online), its specific value influences the slope of the cross-method linear regression. We therefore verify that the reported association does not depend on this choice: across the full plausible range of Filter-imm factors, from $\times 1$ (CF-naive, raw) to $\times 47$, the rank-order Spearman correlation remains in the narrow band $\rho = -0.46$ to -0.58 (Supplement Fig. S7 and Table S9), so the monotonic SIE–INP association is robust to the harmonisation choice and only the magnitude of the linear slope is factor-sensitive. These factors are *not* a calibration transfer and must not be applied unmodified to temperature-resolved slope derivation or absolute-rate trend attribution because the true PINE-vs-method offset is temperature- and aerosol-regime-dependent (Sect. 4.4). A systematic, co-located inter-comparison of these diverse online and offline polar INP observation technologies remains an important focus of our future research.

Here "Filter-imm" denotes the published filter-based immersion-freezing droplet-assay datasets (Wex et al. 2019; Hartmann et al. 2021; Sze et al. 2023) collected at TROPOS-network Arctic stations (Ny-Ålesund and Villum, Greenland), used as INP number-concentration sources in the sea-ice synthesis; the factor of $\times 11.2$ is a concentration-space conversion to the PINE reference scale. Each non-PINE factor is the median PINE/method INP concentration ratio at $T = -20\,^{\circ}\mathrm{C}$ from the

https://doi.org/10.5194/egusphere-2026-3543
Preprint. Discussion started: 6 July 2026

Table A1. Method-specific multiplicative Correction Factors (CF) used or available for placing published INP concentrations on a common PINE-equivalent scale at $T = -20\,^{\circ}\mathrm{C}$ for the multi-dataset sea-ice synthesis (Sect. 3.6). PINE is the reference scale; the factor for each non-PINE method is the median ratio (PINE / method) at the reference temperature.

Method	Multiplicative factor (to PINE scale)	Type	Reference
PINE	1.0	Reference	This study
Filter-imm	11.2	Derived	This study
CSU Ice Spectrometer	1.0	Direct	Creamean et al. (2022)
Filter IS	7	Derived	Barry (2024)
DRINCZ	61	Derived	Li et al. (2025)
DRUM	excluded	—	Barry (2024)

Monte Carlo reference analysis (Fig. A1b). The DRINCZ raw concentration underlying its $\times 61$ factor was digitized from Li et al. (2025) and therefore carries larger uncertainty than the documented Filter IS value (Barry, 2024). DRUM is excluded from the synthesis as detailed above.

External anchor from a co-located online–offline marine inter-comparison

The MC median of ≈ 8 at $T = -20\,^{\circ}\mathrm{C}$ (vs. the fixed CF $= 16$ adopted in the main text) is consistent with the peer-reviewed marine online–offline range documented by Wilbourn et al. (2024), who *simultaneously co-deployed* the online PINE-03 expansion chamber and the offline WT-CRAFT immersion-freezing assay at the Eastern North Atlantic (ENA) Atmospheric Radiation Measurement (ARM) user-facility (Azores) under near-pure marine boundary-layer aerosol conditions, and reported PINE/offline INP concentration ratios spanning approximately 10 to 100 (factor of 10–100) across $T = -25$ to $-15\,^{\circ}\mathrm{C}$ (with a ratio of ≈ 20 at the $T = -20\,^{\circ}\mathrm{C}$ reference temperature, computed from the reported medians $0.40\,\mathrm{L}^{-1}$ vs. $0.02\,\mathrm{L}^{-1}$; underlying datasets archived at Wilbourn and Hiranuma 2023). For continental aerosol regimes, the same authors recovered close agreement at the Southern Great Plains (SGP) ARM site (online–offline ratio ≈ 1, no systematic offset), confirming that the online–offline offset is regime-dependent and reaches its marine-aerosol maximum precisely where the present ARAON observations were taken. Three implications follow.

1. The MC median ratio of ≈ 8 derived here from a pooled, non-co-located PINE-vs-Filter IS comparison lies just below the Wilbourn et al. (2024) empirically established marine range (their PINE/WT-CRAFT ratio reaching ≈ 20 at $T = -20\,^{\circ}\mathrm{C}$), the difference reflecting the lower offline baseline of the WT-CRAFT assay relative to the Filter IS datasets used here; the fixed CF $= 16$ adopted for the multi-dataset sea-ice synthesis sits between the two method-specific estimates. The estimates are therefore mutually consistent in sign and order of magnitude and are anchored by an independent, peer-reviewed, co-located inter-comparison conducted with the same chamber technology (PINE-03).

2. The reported SIE–INP association (Sect. 3.6) is in any case robust to the specific CF value: the rank-order Spearman correlation remains $\rho = -0.46$ to -0.58 across the full Filter-imm CF range ($\times 1$, CF-naive, to $\times 47$; Supplement Fig. S7),

https://doi.org/10.5194/egusphere-2026-3543
Preprint. Discussion started: 6 July 2026

so the monotonic association does not depend on the adopted $\times 11.2$ harmonisation. The MC median offset (≈ 8 for PINE/Filter IS) and the co-located Wilbourn et al. (2024) marine value (≈ 20) both confirm that PINE reads higher than the offline assays in this regime, bracketing the adopted CF $= 16$.

3. The strong temperature dependence of the marine online–offline offset reported by Wilbourn et al. (2024) (their factor ~ 3 at $T = -25\,^{\circ}$C rising to ~ 80 at $T = -15\,^{\circ}$C) independently reproduces the temperature dependence of the PINE/Filter ratio resolved across the bins of Fig. A2, providing a second-order consistency check that any fixed CF, including the CF $= 16$ adopted here, is appropriate only near the $T = -20\,^{\circ}$C reference point and *not* for slope-resolving analyses.

This convergence between the present pooled-dataset MC framework and the Wilbourn et al. (2024) co-located inter-comparison materially strengthens the empirical basis of the harmonisation step beyond what the non-co-located MC analysis alone could provide.

To support the fixed concentration-space CF $= 16$ adopted in the main text (Sect. 4.4), we present here a complementary INP-concentration-space analysis of the PINE-vs-pooled-offline-filter offset and its temperature dependence. This analysis is performed entirely in INP number concentration space (L^{-1}), consistent with the framework used throughout the main text, and is not used in the multi-dataset sea-ice synthesis (Sect. 3.6). Figure A1 shows: (a) $N_{\mathrm{INP}}(T)$ spectra of the PINE Arctic combined dataset against pooled offline filter datasets (Barry 2024 Filter IS / MOSAiC, Li et al. 2025 DRINCZ, Creamean et al. 2022 DRUM / Arctic Century); and (b) the median PINE/method CF ratio per instrument at $T = -20\,^{\circ}$C (16–84 % range shown as error bars), against the adopted CF $= 16$ (95 % range 8–28). The full Monte Carlo ratio distributions at six temperatures (-16 to $-21\,^{\circ}$C), from which these medians and ranges are derived, are shown in Fig. A2; the warmest bins are limited by the number of clean expansion runs available, with $-16\,^{\circ}$C ($n = 14$) the warmest bin retaining sufficient runs for a stable MC estimate (the $-19\,^{\circ}$C value in the ship QC, criterion (4), is a conditional warm-temperature spike-detection threshold, not an analysis cap). The MC percentile envelopes bracket the fixed CF $= 16$ within the 5–95 % range (approximately 2 to 33 at $T = -20\,^{\circ}$C), and the median offset at $T = -20\,^{\circ}$C is approximately 8 — comparable to the Filter IS fixed CF and within the multi-method range (Filter IS ≈ 7 to INAS-D ≈ 120), consistent with the published marine online–offline range (Wilbourn et al., 2024). The temperature dependence of the PINE/Filter ratio evident across the bins of Fig. A2 further confirms the caveat stated in the main text: a single fixed CF is appropriate only for first-order harmonisation near the $T = -20\,^{\circ}$C reference point and must not be applied to temperature-resolved slope derivation or absolute-rate trend attribution. The temperature sensitivity $\beta = \mathrm{d}\log_{10}(N_{\mathrm{INP}})/\mathrm{d}T$ of the PINE Arctic data ($\beta \approx -0.022\,\mathrm{K}^{-1}$ for the campaign-medians; cf. Sect. 2.6) is markedly flatter than the single-location literature compilation (PaCE-2022 September $\beta = -0.087$; Creamean et al. 2022 $\beta = -0.080$; Barry 2024 $\beta \approx -0.073$; Li et al. 2025 $\beta = -0.065$; per-campaign regression statistics in Table S6 in the Supplement).

https://doi.org/10.5194/egusphere-2026-3543
Preprint. Discussion started: 6 July 2026

References

AirKorea: Finalized air quality measurement data, Gosan background monitoring station (Jeju Island, Korea), korea Environment Corporation (K-eco), https://www.airkorea.or.kr, accessed April 2026, 2024.

Atkinson, J. D., Murray, B. J., Woodhouse, M. T., Whale, T. F., Baustian, K. J., Carslaw, K. S., Dobbie, S., O'Sullivan, D., and Malkin, T. L.: The importance of feldspar for ice nucleation by mineral dust in mixed-phase clouds, Nature, 498, 355–358, https://doi.org/10.1038/nature12278, 2013.

Barry, K. R.: Ice nucleating particles in the Arctic: measurement and source tracking, PhD dissertation, Colorado State University, Fort Collins, CO, USA, https://hdl.handle.net/10217/237248, available at Mountain Scholar (Repository ID: islandora:1010323), Ch. 2. Defence: 2023-11-06; advisors: S. Kreidenweis, P. J. DeMott., 2024.

Bigg, E. K. and Leck, C.: Cloud-active particles over the central Arctic Ocean, J. Geophys. Res., 106, 32 155–32 166, https://doi.org/10.1029/1999JD901152, 2001.

Böhmländer, A., Lacher, L., Fösig, R., Büttner, N., Nadolny, J., Brus, D., Doulgeris, K.-M., and Möhler, O.: PaCE-2022 PINE ice-nucleating particle measurements at Sammaltunturi, Finland, Earth Syst. Sci. Data, 17, 6165–6185, https://doi.org/10.5194/essd-17-6165-2025, underlying dataset archived at Zenodo, doi:10.5281/zenodo.16882069, 2025.

Chen, J., Wu, Z., Augustin-Bauditz, S., Grawe, S., Hartmann, M., Pei, X., Liu, Z., Ji, D., and Wex, H.: Ice-nucleating particle concentrations unaffected by urban air pollution in Beijing, China, Atmos. Chem. Phys., 18, 3523–3539, https://doi.org/10.5194/acp-18-3523-2018, 2018.

Creamean, J. M., Kirpes, R. M., Pratt, K. A., Spada, N. J., Maahn, M., de Boer, G., Schnell, R. C., and China, S.: Marine and terrestrial influences on ice nucleating particles during continuous springtime measurements in an Arctic oilfield location, Atmos. Chem. Phys., 18, 18 023–18 042, https://doi.org/10.5194/acp-18-18023-2018, key retained as "Creamean2019" for citation continuity; the paper is the 2018 ACP Oliktok-Point campaign., 2018.

Creamean, J. M., Cross, J. N., Pickart, R., McRaven, L., Lin, P., Pacini, A., Hanlon, R., Schmale, D. G., Ceniceros, J., Aydell, T., Colombi, N., Bolger, E., and DeMott, P. J.: Ice nucleating particles carried from below a phytoplankton bloom to the Arctic atmosphere, Geophys. Res. Lett., 46, 8572–8581, https://doi.org/10.1029/2019GL083039, originally keyed as "Creamean2018" for the Healy icebreaker dataset; the peer-reviewed paper appeared in 2019 (GRL). Key retained to preserve citation continuity., 2019.

Creamean, J. M., Barry, K., Hill, T. C. J., Hume, C., DeMott, P. J., Shupe, M. D., Dahlke, S., Willmes, S., Schmale, J., Beck, I., Hoppe, C. J. M., Fong, A., Chamberlain, E., Bowman, J., Scharien, R., and Persson, O.: Annual cycle observations of aerosols capable of ice formation in central Arctic clouds, Nat. Commun., 13, 3383, https://doi.org/10.1038/s41467-022-31182-x, 2022.

David, R. O., Cascajo-Castresana, M., Brennan, K. P., Rösch, M., Els, N., Werz, J., Weichlinger, V., Boynton, L. S., Bogler, S., Borduas-Dedekind, N., Marcolli, C., and Kanji, Z. A.: Development of the DRoplet Ice Nuclei Counter Zurich (DRINCZ), Atmos. Meas. Tech., 12, 6865–6888, https://doi.org/10.5194/amt-12-6865-2019, 2019.

DeMott, P. J., Prenni, A. J., Liu, X., Kreidenweis, S. M., Petters, M. D., Twohy, C. H., Richardson, M. S., Eidhammer, T., and Rogers, D. C.: Predicting global atmospheric ice nuclei distributions and their impacts on climate, Proc. Natl. Acad. Sci., 107, 11 217–11 222, https://doi.org/10.1073/pnas.0910818107, 2010.

DeMott, P. J., Hill, T. C. J., McCluskey, C. S., Prather, K. A., Collins, D. B., Sullivan, R. C., Ruppel, M. J., Mason, R. H., Irish, V. E., Lee, T., Hwang, C. Y., Rhee, T. S., Snider, J. R., McMeeking, G. R., Dhaniyala, S., Lewis, E. R., Wentzell, J. J. B., Abbatt, J., Lee, C., Sultana, C. M., Ault, A. P., Axson, J. L., Diaz Martinez, M., Venero, I., Santos-Figueroa, G., Stokes, M. D., Deane, G. B., Mayol-Bracero, O. L.,

https://doi.org/10.5194/egusphere-2026-3543
Preprint. Discussion started: 6 July 2026

Grassian, V. H., Bertram, T. H., Bertram, A. K., Moffett, B. F., and Franc, G. D.: Sea spray aerosol as a unique source of ice nucleating particles, Proc. Natl. Acad. Sci., 113, 5797–5803, https://doi.org/10.1073/pnas.1514034112, 2016.

DeMott, P. J., Möhler, O., Cziczo, D. J., Hiranuma, N., Petters, M. D., Petters, S. S., Belosi, F., Bingemer, H. G., Brooks, S. D., Budke, C., Burkert-Kohn, M., Collier, K. N., Danielczok, A., Eppers, O., Felgitsch, L., Garimella, S., Grothe, H., Herenz, P., Hill, T. C. J., Höhler, K., Kanji, Z. A., Kiselev, A., Koop, T., Kristensen, T. B., Krüger, K., Kulkarni, G., Levin, E. J. T., Murray, B. J., Nicosia, A., O'Sullivan, D., Peckhaus, A., Polen, M. J., Price, H. C., Reicher, N., Rothenberg, D. A., Rudich, Y., Santachiara, G., Schiebel, T., Schrod, J., Seifried, T. M., Stratmann, F., Sullivan, R. C., Suski, K. J., Szakall, M., Taylor, H. P., Ullrich, R., Vergara-Temprado, J., Wagner, R., Whale, T. F., Weber, D., Welti, A., Whiteside, C. L., Wright, T. P., and Yakobi-Hancock, J. D.: The Fifth International Workshop on Ice Nucleation phase 2 (FIN-02): laboratory intercomparison of ice nucleation measurements, Atmos. Meas. Tech., 11, 6231–6257, https://doi.org/10.5194/amt-11-6231-2018, 2018.

Gong, X., Wex, H., Voigtländer, J., Fomba, K. W., Müller, K., Henning, S., Triesch, N., Welti, A., van Pinxteren, M., Hoffmann, T., Wille, M., Stratmann, F., and Herrmann, H.: Characterization of aerosol particles at Cabo Verde close to sea level and at the cloud level – Part 2: Ice-nucleating particles in air, cloud and seawater, Atmos. Chem. Phys., 20, 1451–1468, https://doi.org/10.5194/acp-20-1451-2020, 2020.

Hartmann, M., Gong, X., Kecorius, S., van Pinxteren, M., Vogl, T., Welti, A., Wex, H., Zeppenfeld, S., Herrmann, H., Wiedensohler, A., and Stratmann, F.: Terrestrial or marine – indications towards the origin of ice-nucleating particles during melt season in the European Arctic up to 83.7°N, Atmos. Chem. Phys., 21, 11 613–11 636, https://doi.org/10.5194/acp-21-11613-2021, 2021.

Ickes, L., Porter, G. C. E., Wagner, R., Adams, M. P., Bierbauer, S., Bertram, A. K., Bilde, M., Christiansen, S., Ekman, A. M. L., Gorokhova, E., Höhler, K., Kiselev, A. A., Leck, C., Möhler, O., Murray, B. J., Schiebel, T., Ullrich, R., and Salter, M. E.: The ice-nucleating activity of Arctic sea surface microlayer samples and marine algal cultures, Atmos. Chem. Phys., 20, 11 089–11 117, https://doi.org/10.5194/acp-20-11089-2020, 2020.

Irish, V. E., Hanna, S. J., Yu, X., Boyer, M., Polishchuk, E., Ahmed, M., Chen, J., Abbatt, J. P. D., Gosselin, M., and Chang, R. Y.-W.: Revisiting properties and concentrations of ice-nucleating particles in the sea surface microlayer and bulk seawater in the Canadian Arctic during summer, Atmos. Chem. Phys., 19, 7775–7787, https://doi.org/10.5194/acp-19-7775-2019, 2019.

Iwata, A. and Matsuki, A.: Characterization of individual ice residual particles by the single droplet freezing method: a case study in the Asian dust outflow region, Atmos. Chem. Phys., 18, 1785–1804, https://doi.org/10.5194/acp-18-1785-2018, key retained as "Iwata2022" for citation continuity; the only Iwata + Matsuki Asian-dust INP paper found in the literature is the 2018 ACP study., 2018.

Kanji, Z. A., Ladino, L. A., Wex, H., Boose, Y., Burkert-Kohn, M., Cziczo, D. J., and Krämer, M.: Overview of ice nucleating particles, Meteorol. Monogr., 58, 1.1–1.33, https://doi.org/10.1175/AMSMONOGRAPHS-D-16-0006.1, 2017.

Kawai, K., Matsui, H., and Tobo, Y.: Dominant Role of Arctic Dust With High Ice Nucleating Ability in the Arctic Lower Troposphere, Geophys. Res. Lett., 50, e2022GL102 470, https://doi.org/10.1029/2022GL102470, 2023.

Lacher, L., Adams, M. P., Barry, K., Bertozzi, B., Bingemer, H., Boffo, C., Bras, Y., Büttner, N., Castarede, D., Cziczo, D. J., DeMott, P. J., Fösig, R., Goodell, M., Höhler, K., Hill, T. C. J., Jentzsch, C., Ladino, L. A., Levin, E. J. T., Mertes, S., Möhler, O., Moore, K. A., Murray, B. J., Nadolny, J., Pfeuffer, T., Picard, D., Ramírez-Romero, C., Ribeiro, M., Richter, S., Schrod, J., Sellegri, K., Stratmann, F., Swanson, B. E., Thomson, E. S., Wex, H., Wolf, M. J., and Freney, E.: The Puy de Dôme ICe Nucleation Intercomparison Campaign (PICNIC): comparison between online and offline methods in ambient air, Atmos. Chem. Phys., 24, 2651–2678, https://doi.org/10.5194/acp-24-2651-2024, 2024.

https://doi.org/10.5194/egusphere-2026-3543
Preprint. Discussion started: 6 July 2026

Li, G., Welti, A., Rocchi, A., Pérez Fogwill, G., Dall'Osto, M., and Kanji, Z. A.: Terrestrial and marine sources of ice nucleating particles in the Eurasian Arctic, Faraday Discuss., 258, 94, https://doi.org/10.1039/D4FD00160E, arctic Century Expedition 2021 (Barents/Kara/Laptev seas) shipborne INP measurements using the DRINCZ offline and HINC online assays., 2025.

McCluskey, C. S., Hill, T. C. J., Sultana, C. M., Laskina, O., Trueblood, J., Santander, M. V., Beall, C. M., Michaud, J. M., Kreidenweis, S. M., Prather, K. A., Grassian, V., and DeMott, P. J.: A Mesocosm Double Feature: Insights into the Chemical Makeup of Marine Ice Nucleating Particles, J. Atmos. Sci., 75, 2405–2423, https://doi.org/10.1175/JAS-D-17-0155.1, 2018.

Meyers, M. P., DeMott, P. J., and Cotton, W. R.: New primary ice-nucleation parameterizations in an explicit cloud model, J. Appl. Meteorol., 31, 708–721, https://doi.org/10.1175/1520-0450(1992)031<0708:NPINPI>2.0.CO;2, 1992.

Modini, R. L., Frossard, A. A., Ahlm, L., Russell, L. M., Corrigan, C. E., Roberts, G. C., Hawkins, L. N., Schroder, J. C., Bertram, A. K., Zhao, R., Lee, A. K. Y., Abbatt, J. P. D., Lin, J., Nenes, A., Wang, Z., Wonaschütz, A., Sorooshian, A., Noone, K. J., Jonsson, H., Seinfeld, J. H., Toom-Sauntry, D., Macdonald, A. M., and Leaitch, W. R.: Primary marine aerosol-cloud interactions off the coast of California, J. Geophys. Res. Atmos., 120, 4282–4303, https://doi.org/10.1002/2014JD022963, 2015.

Möhler, O., Adams, M., Lacher, L., Vogel, F., Nadolny, J., Ullrich, R., Boffo, C., Pfeuffer, T., Hobl, A., Weiß, M., Vepuri, H. S. K., Hiranuma, N., and Murray, B. J.: The portable ice nucleation experiment (PINE): a new online instrument for laboratory studies and automated long-term field observations of ice-nucleating particles, Atmos. Meas. Tech., 14, 1143–1166, https://doi.org/10.5194/amt-14-1143-2021, 2021.

Murray, B. J., O'Sullivan, D., Atkinson, J. D., and Webb, M. E.: Ice nucleation by particles immersed in supercooled cloud droplets, Chem. Soc. Rev., 41, 6519–6554, https://doi.org/10.1039/c2cs35200a, 2012.

National Snow and Ice Data Center (NSIDC): Sea Ice Index, Version 3, boulder, Colorado USA. NSIDC: National Snow and Ice Data Center. https://doi.org/10.7265/N5K072F8, 2024.

National Snow and Ice Data Center (NSIDC): Sea Ice Index, Version 3, boulder, Colorado USA. NSIDC: National Snow and Ice Data Center. https://doi.org/10.7265/N5K072F8, 2025.

Newey, W. K. and West, K. D.: A Simple, Positive Semi-Definite, Heteroskedasticity and Autocorrelation Consistent Covariance Matrix, Econometrica, 55, 703–708, https://doi.org/10.2307/1913610, 1987.

Pasquier, J. T., Henneberger, J., Ramelli, F., Lauber, A., David, R. O., Wieder, J., Carlsen, T., Gierens, R., Maturilli, M., and Lohmann, U.: Conditions favorable for secondary ice production in Arctic mixed-phase clouds, Atmos. Chem. Phys., 22, 15 579–15 601, https://doi.org/10.5194/acp-22-15579-2022, 2022.

Porter, G. C. E., Adams, M. P., Brooks, I. M., Ickes, L., Karlsson, L., Leck, C., Salter, M. E., Schmale, J., Siegel, K., Sikora, S. N. F., Tarn, M. D., Vüllers, J., Wernli, H., Zieger, P., Zinke, J., and Murray, B. J.: Highly active ice-nucleating particles at the summer North Pole, J. Geophys. Res. Atmos., 127, e2021JD036 059, https://doi.org/10.1029/2021JD036059, 2022.

Price, H. C., Baustian, K. J., McQuaid, J. B., Blyth, A., Bower, K. N., Choularton, T., Cotton, R. J., Cui, Z., Field, P. R., Gallagher, M., Hawker, R., Merrington, A., Miltenberger, A., Neely III, R. R., Parker, S. T., Rosenberg, P. D., Taylor, J. W., Trembath, J., Vergara-Temprado, J., Whale, T. F., Wilson, T. W., Young, G., and Murray, B. J.: Atmospheric ice-nucleating particles in the dusty tropical Atlantic, J. Geophys. Res. Atmos., 123, 2175–2193, https://doi.org/10.1002/2017JD027560, 2018.

Sanchez-Marroquin, A., Arnalds, O., Baustian-Dorsi, K. J., Browse, J., Dagsson-Waldhauserova, P., Harrison, A. D., Maters, E. C., Pringle, K. J., Vergara-Temprado, J., Burke, I. T., McQuaid, J. B., Carslaw, K. S., and Murray, B. J.: Iceland is an episodic source of atmospheric ice-nucleating particles relevant for mixed-phase clouds, Sci. Adv., 6, eaba8137, https://doi.org/10.1126/sciadv.aba8137, 2020.

https://doi.org/10.5194/egusphere-2026-3543
Preprint. Discussion started: 6 July 2026

Säntl-Temkiv, T., Lange, R., Beddows, D., Rauter, U., Pilgaard, S., Dall'Osto, M., Gunde-Cimerman, N., Massling, A., and Wex, H.: Biogenic sources of ice nucleating particles at the high Arctic, Environ. Sci. Technol., 53, 8238–8247, https://doi.org/10.1021/acs.est.9b00991, 2019.

Schmale, J., Zieger, P., and Ekman, A. M. L.: Aerosols in current and future Arctic climate, Nat. Clim. Change, 11, 95–105, https://doi.org/10.1038/s41558-020-00969-5, 2021.

Shi, Y. and Liu, X.: Dust radiative effects on climate by glaciating mixed-phase clouds, Geophys. Res. Lett., 46, 6128–6137, https://doi.org/10.1029/2019GL082504, 2019.

Sze, K. C. H., Wex, H., Hartmann, M., Skov, H., Massling, A., Villanueva, D., and Stratmann, F.: Ice-nucleating particles in northern Greenland: annual cycles, biological contribution and parameterizations, Atmos. Chem. Phys., 23, 4741–4761, https://doi.org/10.5194/acp-23-4741-2023, 2023.

Tan, I. and Storelvmo, T.: Evidence of strong contributions from mixed-phase clouds to Arctic climate change, Geophys. Res. Lett., 46, 2894–2902, https://doi.org/10.1029/2018GL081871, 2019.

Tan, I., Storelvmo, T., and Zelinka, M. D.: Observational constraints on mixed-phase clouds imply higher climate sensitivity, Science, 352, 224–227, https://doi.org/10.1126/science.aad5300, 2016.

Tatzelt, C., Henning, S., Welti, A., Baccarini, A., Hartmann, M., Gysel-Beer, M., van Pinxteren, M., Modini, R. L., Schmale, J., and Stratmann, F.: Circum-Antarctic abundance and properties of CCN and INPs, Atmos. Chem. Phys., 22, 9721–9745, https://doi.org/10.5194/acp-22-9721-2022, 2022.

Tobo, Y., DeMott, P. J., Hill, T. C. J., Prenni, A. J., Swoboda-Colberg, N. G., Franc, G. D., and Kreidenweis, S. M.: Biological aerosol particles as a key determinant of ice nuclei populations in a forest ecosystem, J. Geophys. Res. Atmos., 118, 10 100–10 110, https://doi.org/10.1002/jgrd.50801, 2013.

Tobo, Y., Adachi, K., DeMott, P. J., Hill, T. C. J., Hamilton, D. S., Mahowald, N. M., Nagatsuka, N., Ohata, S., Uetake, J., Kondo, Y., and Koike, M.: Glacially sourced dust as a potentially significant source of ice nucleating particles, Nat. Geosci., 12, 253–258, https://doi.org/10.1038/s41561-019-0314-x, key retained as "Tobo2020" for citation continuity; the paper was published online December 2019., 2019.

Uno, I., Eguchi, K., Yumimoto, K., Takemura, T., Shimizu, A., Uematsu, M., Liu, Z., Wang, Z., Hara, Y., and Sugimoto, N.: Asian dust transported one full circuit around the globe, Nat. Geosci., 2, 557–560, https://doi.org/10.1038/ngeo583, 2009.

Vepuri, H. S. K., Rodríguez, C. A., Georgakopoulos, D. G., Hume, D., Webb, J., Mayer, G. D., and Hiranuma, N.: Ice-nucleating particles in precipitation samples from the Texas Panhandle, Atmos. Chem. Phys., 21, 4503–4520, https://doi.org/10.5194/acp-21-4503-2021, 2021.

Vergara-Temprado, J., Murray, B. J., Wilson, T. W., O'Sullivan, D., Browse, J., Pringle, K. J., Ardon-Dryer, K., Bertram, A. K., Burrows, S. M., Ceburnis, D., DeMott, P. J., Mason, R. H., O'Dowd, C. D., Rinaldi, M., and Carslaw, K. S.: Contribution of feldspar and marine organic aerosols to global ice nucleating particle concentrations, Atmos. Chem. Phys., 17, 3637–3658, https://doi.org/10.5194/acp-17-3637-2017, 2017.

Vergara-Temprado, J., Miltenberger, A. K., Furtado, K., Grosvenor, D. P., Shipway, B. J., Hill, A. A., Wilkinson, J. M., Field, P. R., Murray, B. J., and Carslaw, K. S.: Strong control of Southern Ocean cloud reflectivity by ice-nucleating substances, Proc. Natl. Acad. Sci., 115, 2687–2692, https://doi.org/10.1073/pnas.1721627115, 2018.

Welti, A., Bigg, E. K., DeMott, P. J., Gong, X., Hartmann, M., Harvey, M., Henning, S., Herenz, P., Hill, T. C. J., Hornblow, B., Leck, C., Löffler, M., McCluskey, C. S., Rauker, A. M., Schmale, J., Tatzelt, C., van Pinxteren, M., and Stratmann, F.: Ship-based measure-

https://doi.org/10.5194/egusphere-2026-3543
Preprint. Discussion started: 6 July 2026

ments of ice nuclei concentrations over the Arctic, Atlantic, Pacific and Southern oceans, Atmos. Chem. Phys., 20, 15 191–15 206, https://doi.org/10.5194/acp-20-15191-2020, 2020.

Wex, H., Huang, L., Zhang, W., Hung, H., Traversi, R., Becagli, S., Sheesley, R. J., Moffett, C. E., Barrett, T. E., Bossi, R., Skov, H., Hünerbein, A., Lubitz, J., Löffler, M., Linke, O., Hartmann, M., Herenz, P., and Stratmann, F.: Annual variability of ice-nucleating particle concentrations at different Arctic locations, Atmos. Chem. Phys., 19, 5293–5311, https://doi.org/10.5194/acp-19-5293-2019, 2019.

Wilbourn, E. K. and Hiranuma, N.: Abundance of ice-nucleating particles and cloud condensation nuclei measured at the Southern Great Plains and Eastern North Atlantic observatories in autumn 2019 and 2020, PANGAEA, https://doi.org/10.1594/PANGAEA.964038, cC-BY-4.0 licence; bundled publication of 14 datasets, 2023.

Wilbourn, E. K., Thornton, D. C. O., Ott, C., Graff, J., Quinn, P. K., Bates, T. S., Betha, R., Russell, L. M., Behrenfeld, M. J., and Brooks, S. D.: Ice nucleation by marine aerosols over the North Atlantic Ocean in late spring, J. Geophys. Res. Atmos., 125, e2019JD030 913, https://doi.org/10.1029/2019JD030913, 2020.

Wilbourn, E. K., Lacher, L., Guerrero, C., Vepuri, H. S. K., Höhler, K., Nadolny, J., Pantoya, A. D., Möhler, O., and Hiranuma, N.: Measurement report: A comparison of ground-level ice-nucleating-particle abundance and aerosol properties during autumn at contrasting marine and terrestrial locations, Atmos. Chem. Phys., 24, 5433–5456, https://doi.org/10.5194/acp-24-5433-2024, 2024.

Willis, M. D., Leaitch, W. R., and Abbatt, J. P. D.: Processes controlling the composition and abundance of Arctic aerosol, Rev. Geophys., 56, 621–671, https://doi.org/10.1029/2018RG000602, 2018.

Wilson, T. W., Ladino, L. A., Alpert, P. A., Breckels, M. N., Brooks, I. M., Browse, J., Burrows, S. M., Carslaw, K. S., Huffman, J. A., Judd, C., Kilthau, W. P., Mason, R. H., McFiggans, G., Miller, L. A., Nájera, J. J., Polishchuk, E., Rae, S., Schiller, C. L., Si, M., Vergara-Temprado, J., Whale, T. F., Wong, J. P. S., Wurl, O., Yakobi-Hancock, J. D., Abbatt, J. P. D., Aller, J. Y., Bertram, A. K., Knopf, D. A., and Murray, B. J.: A marine biogenic source of atmospheric ice-nucleating particles, Nature, 525, 234–238, https://doi.org/10.1038/nature14986, 2015.

Zeppenfeld, S., van Pinxteren, M., Hartmann, M., Bracher, A., Stratmann, F., and Herrmann, H.: Glucose as a Potential Chemical Marker for Ice Nucleating Activity in Arctic Seawater and Melt Pond Samples, Environ. Sci. Technol., 53, 8747–8756, https://doi.org/10.1021/acs.est.9b01469, 2019.

https://doi.org/10.5194/egusphere-2026-3543
Preprint. Discussion started: 6 July 2026

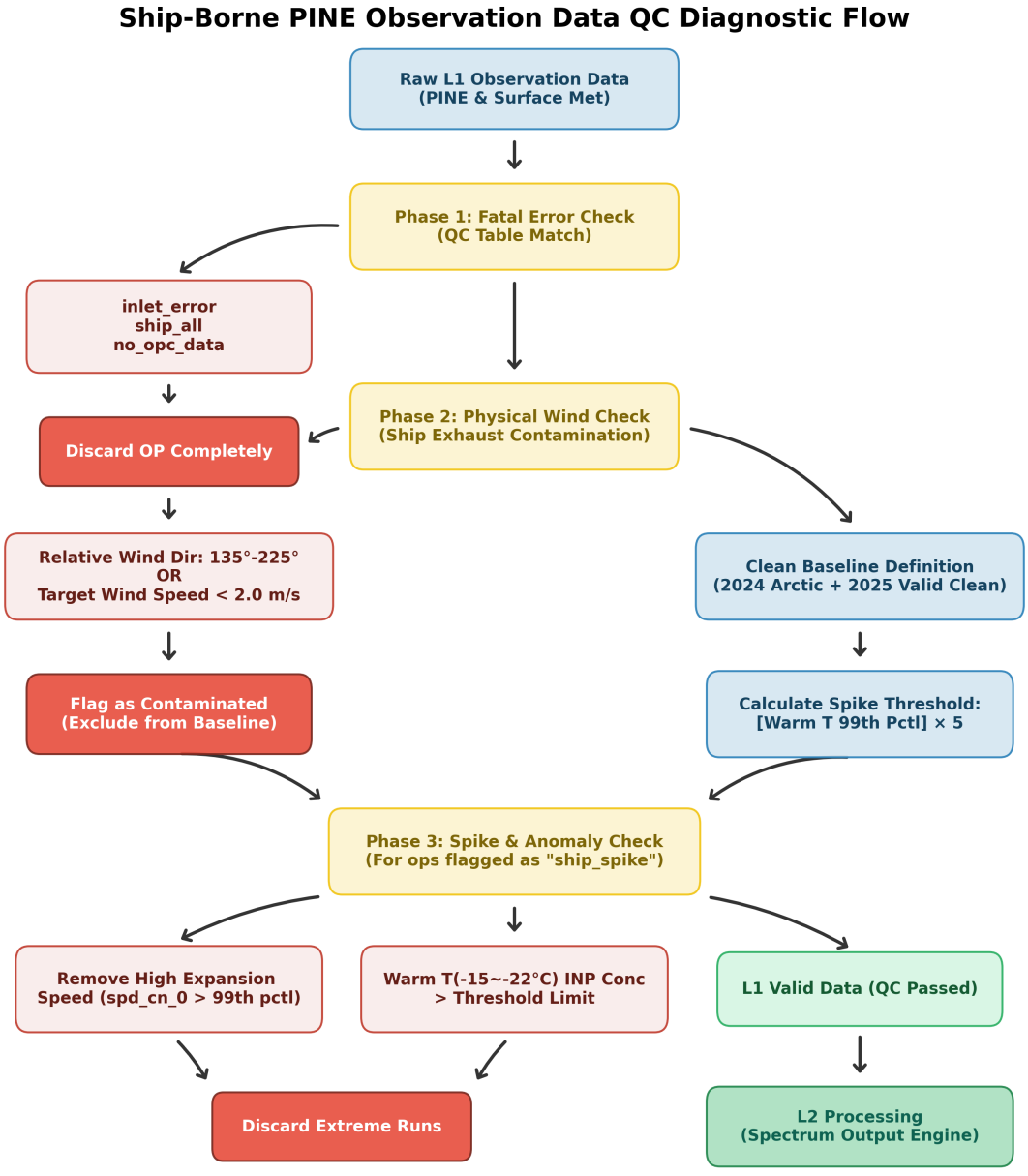

Figure 1. Flowchart of the shipborne PINE observation data quality control (QC) procedure. Phase 1 identifies fatal errors (inlet malfunction, complete ship contamination, missing POPS data). Phase 2 applies physical wind-direction and wind-speed filters to flag exhaust-contaminated runs. Phase 3 performs spike and anomaly detection on partially contaminated operations. Runs passing all phases are classified as L1 valid data for spectral analysis.

https://doi.org/10.5194/egusphere-2026-3543
Preprint. Discussion started: 6 July 2026

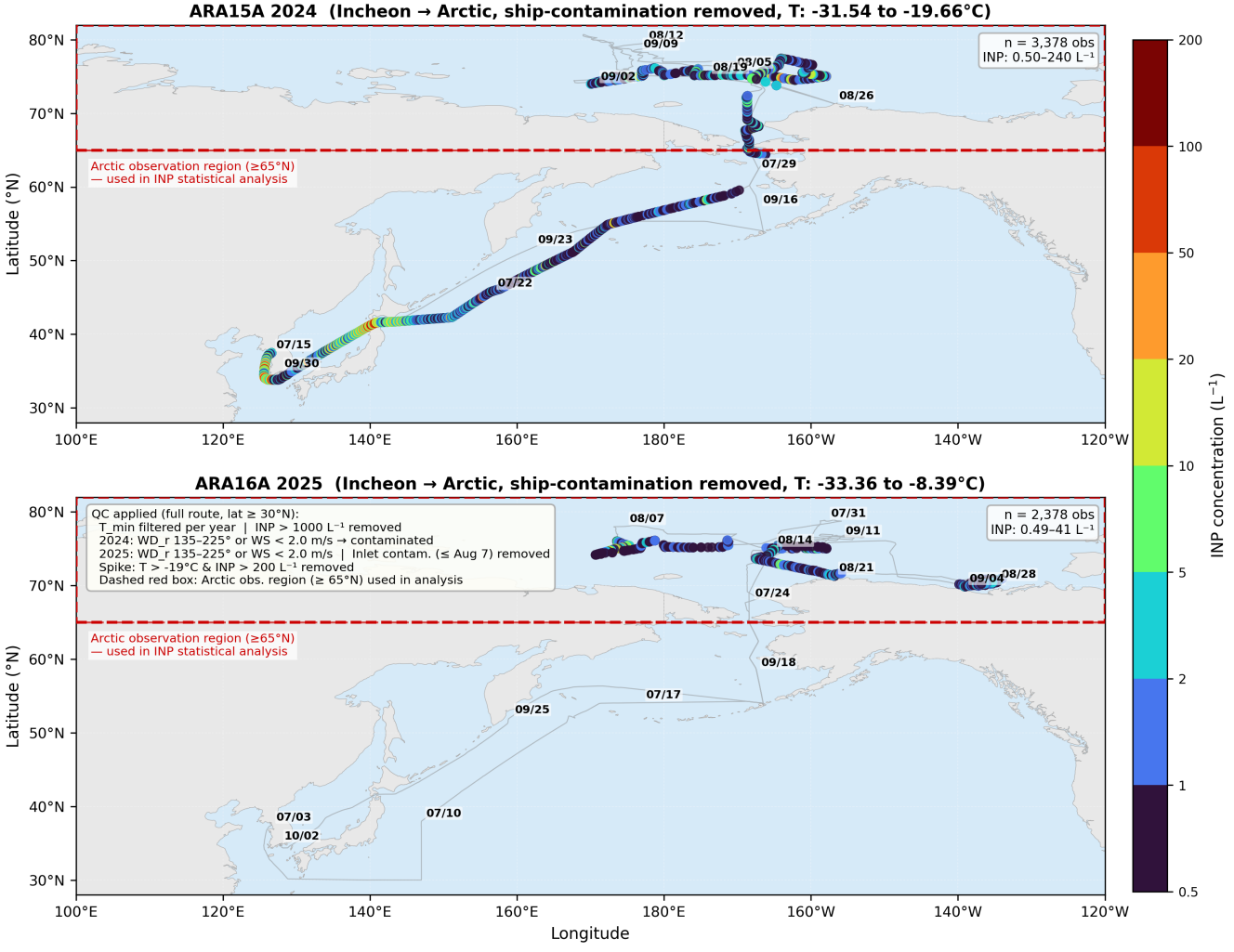

Figure 2. Cruise tracks and INP concentrations measured aboard RV Araon during ARA15A (2024, upper panel) and ARA16A (2025, lower panel). Coloured circles denote individual PINE expansion runs, colour-coded by INP concentration on a logarithmic scale (L^{-1}). Ship-contamination-flagged runs have been removed. Date labels indicate key waypoints along each transect.

https://doi.org/10.5194/egusphere-2026-3543
Preprint. Discussion started: 6 July 2026

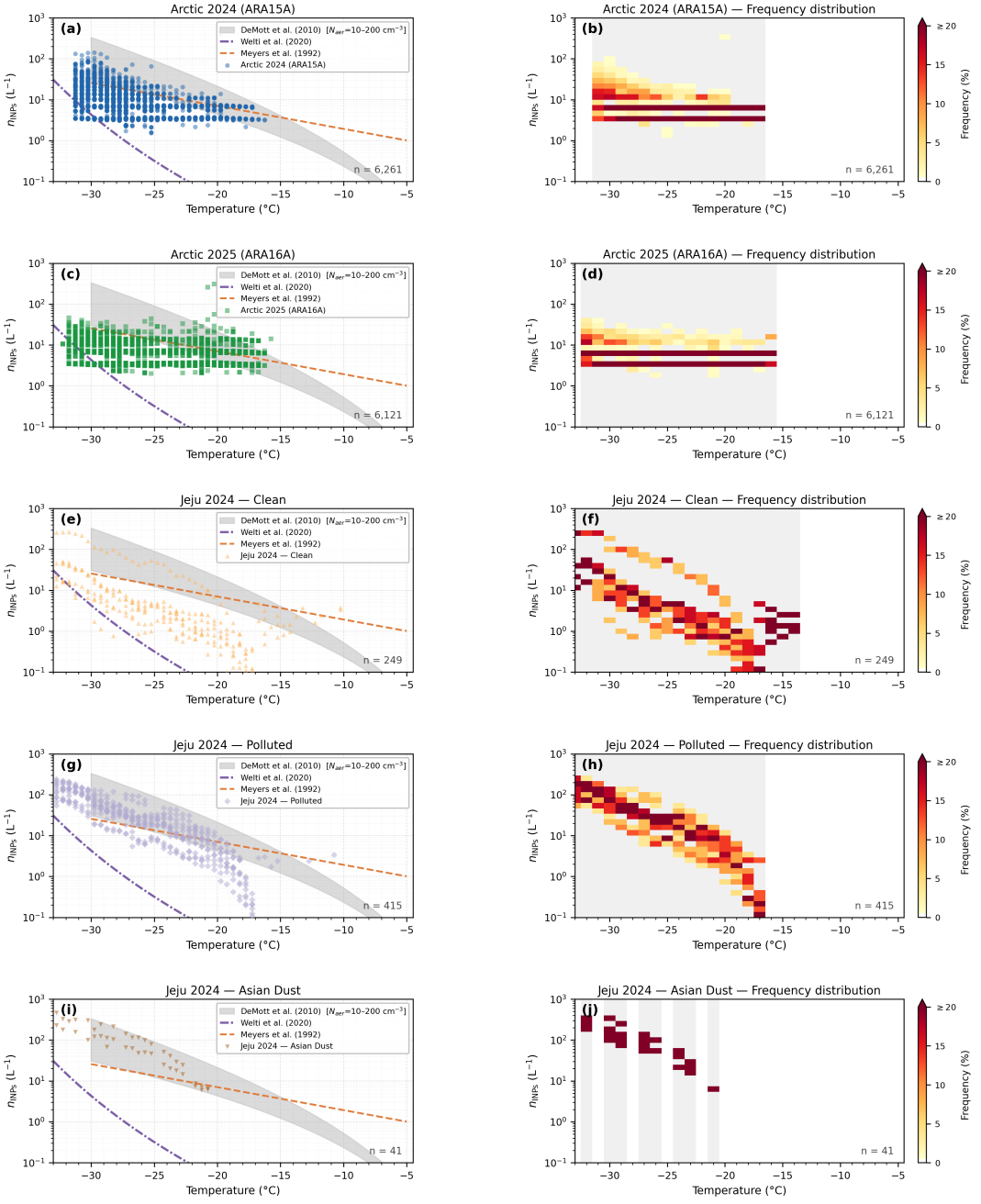

Figure 3. INP temperature spectra (left, scatter) and frequency distributions (right, heatmap) for Arctic and Jeju datasets. (a, b) Arctic 2024 (ARA15A), (c, d) Arctic 2025 (ARA16A), (e, f) Jeju Clean, (g, h) Jeju Polluted, (i, j) Jeju Asian Dust. Scatter plots overlay parameterisation curves (DeMott et al. (2010) envelope, Welti et al. (2020) median, Meyers et al. (1992)). Frequency histograms show percentage per temperature–concentration bin. All panels use common axes for direct comparison.

https://doi.org/10.5194/egusphere-2026-3543
Preprint. Discussion started: 6 July 2026

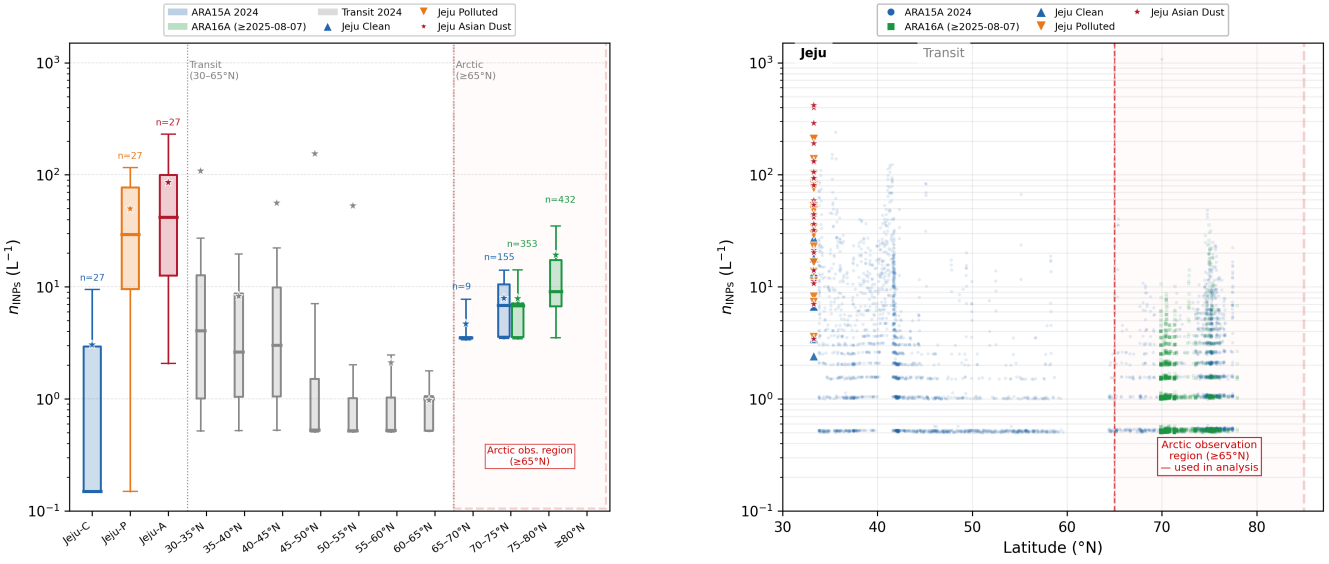

Figure 4. Latitudinal distribution of INP concentrations along the full RV Araon cruise track (Incheon, Korea, ≈37° N, to the Arctic Ocean) and at Jeju Island. (Left) Box-and-whisker plots (Q10–Q25–median–Q75–Q90; star = mean) grouped into three sections: Jeju Island sub-categories (Clean, Polluted, Asian Dust; all at ≈33° N); transit latitude bands (30–35° N through 60–65° N, grey/blue); and Arctic latitude bands (65–70° N, 70–75° N, 75–80° N, ≥80° N). All data are filtered to the common temperature range −18.0 to −31.5 °C. The dashed red box marks the Arctic observation region (≥65° N), which constitutes the primary analysis domain for the Arctic INP statistics reported in this study. (Right) Individual PINE runs plotted against continuous latitude (30–87° N) for ARA15A 2024 and ARA16A 2025, with Jeju event categories overlaid at 33.25° N. The dashed red box and vertical dashed line at 65° N delineate the Arctic observation region used in Sects. 3.1–3.3 and 3.5.

https://doi.org/10.5194/egusphere-2026-3543
Preprint. Discussion started: 6 July 2026

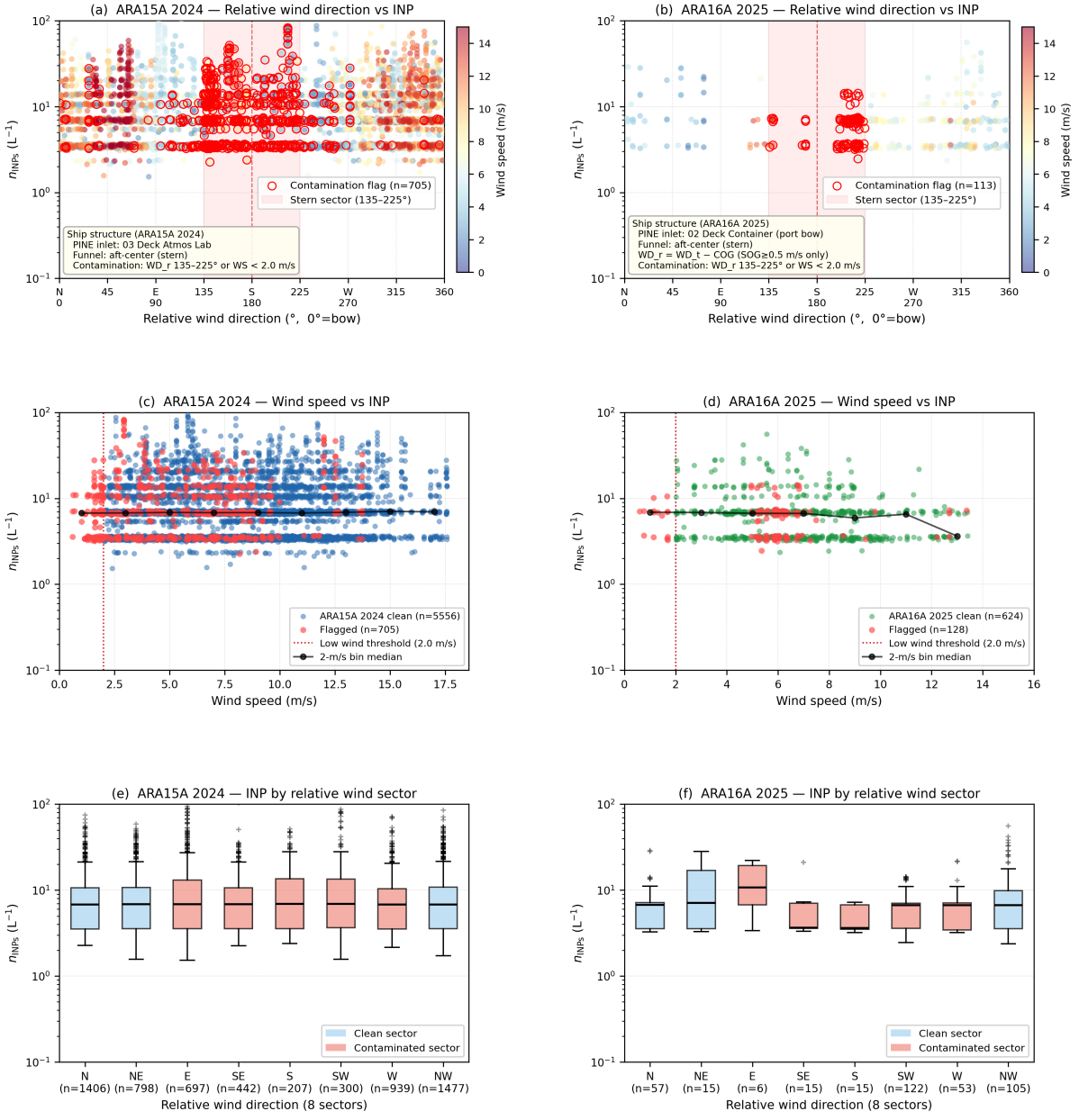

Figure 5. Ship exhaust contamination diagnostics for ARA15A 2024 (left column) and ARA16A 2025 (right column). (a, b) INP concentration versus relative wind direction (WD_r, 0° = bow); red-shaded area marks the stern sector (135–225°); open circles denote contamination-flagged runs. For ARA16A 2025, WD_r was derived as $WD_t - COG$ (mod 360°) using the ARAON_DADIS_GPS_ARCTIC_2025 navigation dataset; points with SOG < 0.5 m s^{-1} lack a WD_r estimate and are excluded from panel (b). (c, d) INP concentration versus wind speed; vertical dashed line marks the 2.0 m s^{-1} low-wind threshold. (e, f) Box-and-whisker comparison of INP concentrations by 8-sector relative wind direction for clean (blue) and contaminated (pink) sectors.

https://doi.org/10.5194/egusphere-2026-3543
Preprint. Discussion started: 6 July 2026

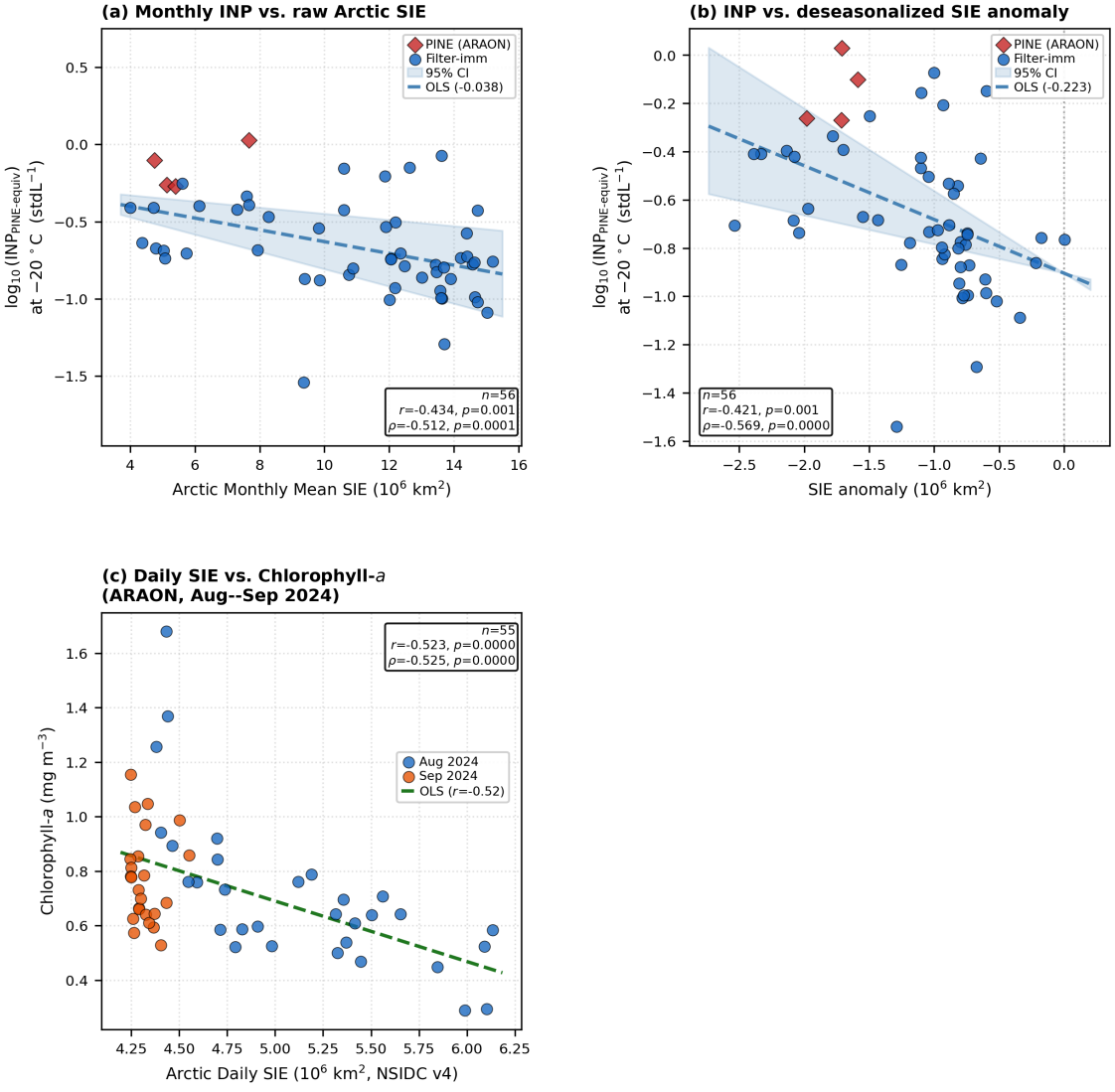

Figure 6. Arctic sea-ice extent (SIE), INP concentrations, and surface Chlorophyll-a synthesis. (a) Monthly Arctic SIE vs. $\log_{10}$(INP) at $T = -20\,^{\circ}$C from eight datasets spanning 2012–2025 ($n = 56$ dataset-month pairs); INP shown with the offline Filter-imm subset harmonised to the PINE concentration scale (Filter-imm $\times 11.2$, PINE $\times 1$; Appendix A) at the $T = -20\,^{\circ}$C reference temperature, where method-specific online–offline offsets are smallest (Sect. 4.4); sensitivity of the regression to this harmonisation factor is documented in Supplement Fig. S7. (b) Deseasonalised SIE anomaly vs. $\log_{10}$(INP); dashed line is the OLS regression (Spearman $\rho = -0.57$, $p < 0.001$; Newey–West HAC-corrected slope -0.22, 95 % CI $[-0.36, -0.09]$). (c) Daily Arctic SIE vs. surface Chlorophyll-a in the central Arctic during August–September 2024 ($n = 55$; Pearson $r = -0.52$, $p < 0.001$); blue = August, orange = September.

https://doi.org/10.5194/egusphere-2026-3543
Preprint. Discussion started: 6 July 2026

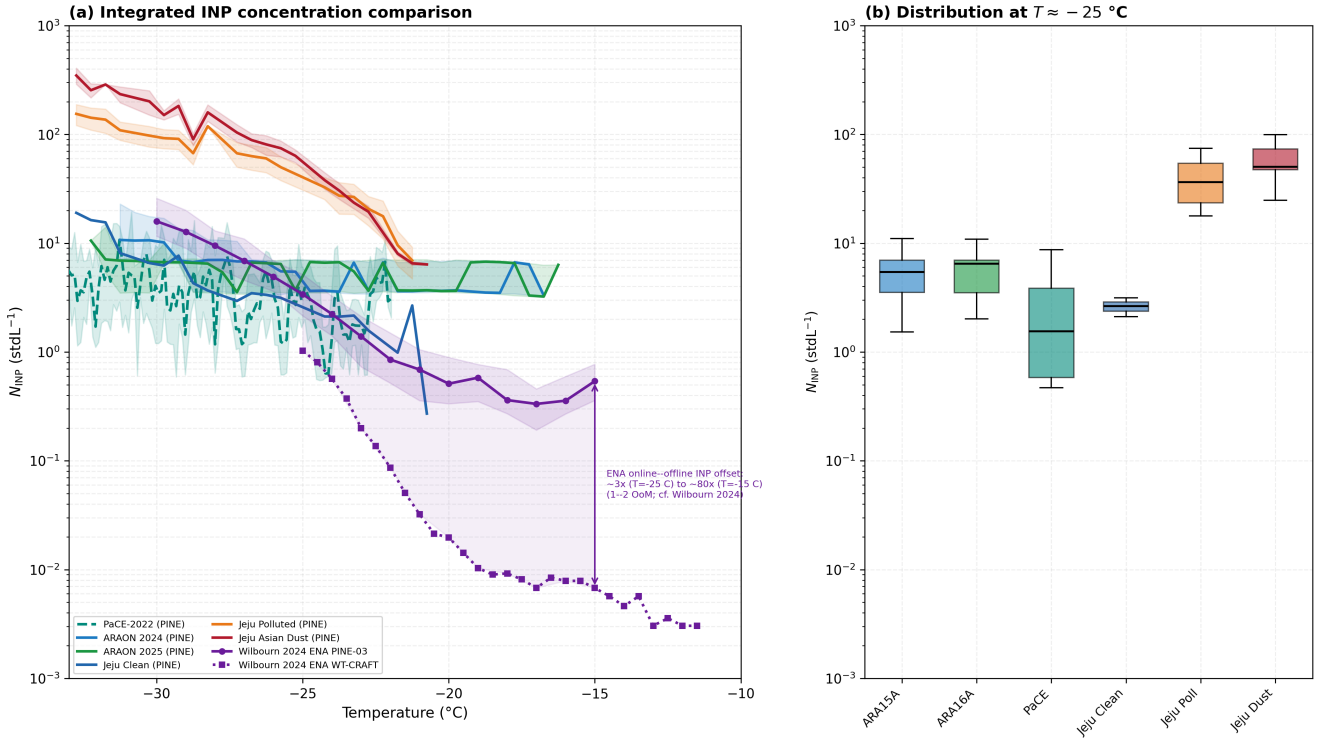

Figure 7. Integrated comparison of INP number concentration $N_{\mathrm{INP}}(T)$ from multiple PINE campaigns. (a) Temperature spectra for ARAON Arctic (2024, 2025), PaCE-2022 (Sammaltunturi, Böhmländer et al. 2025), and Jeju sub-categories (Clean, Polluted, Asian Dust), with the marine online–offline pair from the Wilbourn et al. (2024) ENA campaign overlaid (PINE-03 chamber, solid purple with circles; WT-CRAFT polycarbonate-filter offline assay, dotted purple with squares; the light purple band between the two curves visualises the marine online–offline INP concentration offset, which evolves from a factor of ∼3 at $T = -25\,^{\circ}\mathrm{C}$ to a factor of ∼80 at $T = -15\,^{\circ}\mathrm{C}$, consistent with the "1–2 orders of magnitude" marine discrepancy reported in Wilbourn et al. 2024 Sect. 3). Solid/dashed lines are temperature-bin medians; shaded bands denote the 25th–75th percentile range. Notably, the real-time ARAON spectra remain comparatively flat, with little decline in N_{INP} toward warm temperatures (-20 to $-15\,^{\circ}\mathrm{C}$), in contrast to the steeper warm-temperature fall-off of the offline-filter Arctic Ocean record — reflecting warm-active marine-biogenic INP that integrated filter sampling tends to underestimate (Sect. 4.4). (b) Box-and-whisker comparison of N_{INP} distributions across all PINE datasets at $T \approx -25\,^{\circ}\mathrm{C}$. A site-resolved supplementary comparison (continental SGP vs. marine ENA, PINE-03 vs. co-located offline assays; data from Wilbourn et al. 2024 via PANGAEA, 10.1594/PANGAEA.964038) is provided in Fig. S6 in the Supplement.

https://doi.org/10.5194/egusphere-2026-3543
Preprint. Discussion started: 6 July 2026

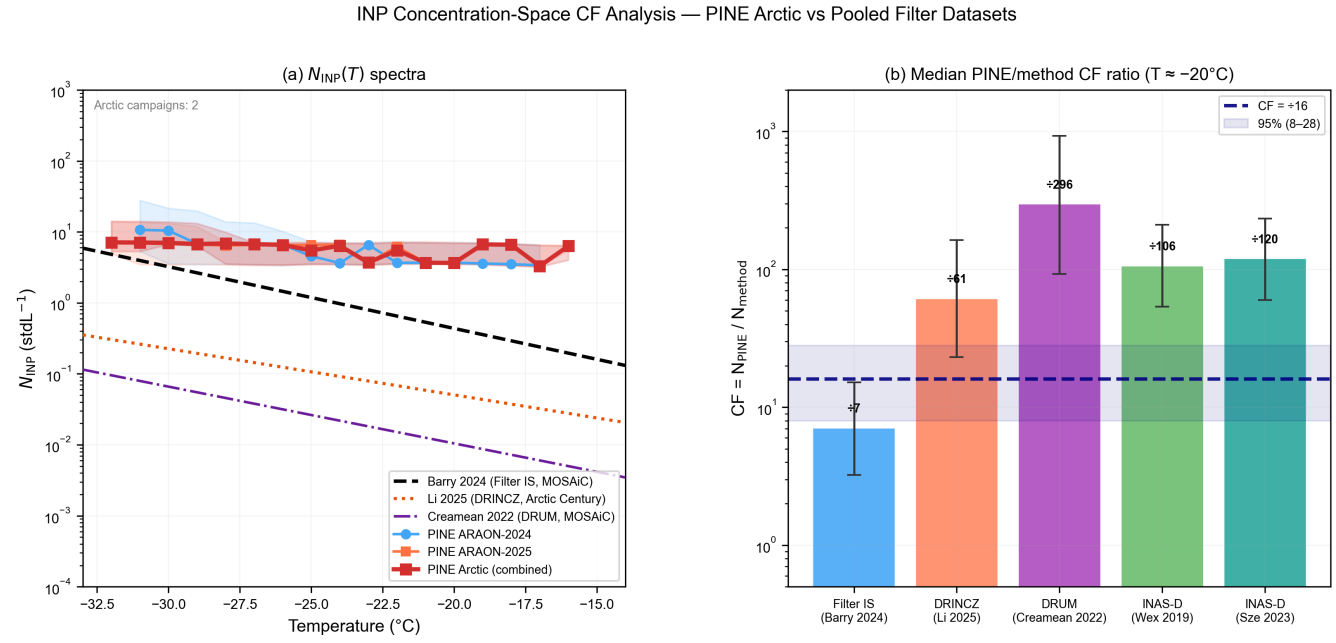

Figure A1. INP-concentration-space cross-check on the fixed CF = 16 adopted in the main text (Sect. 4.4). (a) $N_{\mathrm{INP}}(T)$ spectra: PINE Arctic combined (red) compared with the pooled offline filter datasets (Barry, 2024; Li et al., 2025; Creamean et al., 2022) on their raw (reported) concentration scale. (b) Median PINE/method INP concentration ratio at $T = -20\,^{\circ}\mathrm{C}$ for each offline method (Barry 2024 Filter IS ≈ 7, Li et al. 2025 DRINCZ ≈ 61, Creamean et al. 2022 DRUM ≈ 296, Wex et al. 2019; Sze et al. 2023 INAS-D ≈ 106–120; bars with 16–84 % range), shown against the adopted CF = 16 (dashed line) and its 95 % range (8–28; shaded band); the median PINE/Filter IS ratio (≈ 8, 16–84 % range ≈ 4–19) brackets the adopted CF, while the large DRUM offset motivates its exclusion from the multi-dataset sea-ice synthesis (Sect. 3.6). The temperature-resolved Monte Carlo distributions underlying these medians are shown in Fig. A2. This INP-space analysis supports the concentration-space framework and is not used in the sea-ice synthesis (Sect. 3.6).

https://doi.org/10.5194/egusphere-2026-3543
Preprint. Discussion started: 6 July 2026

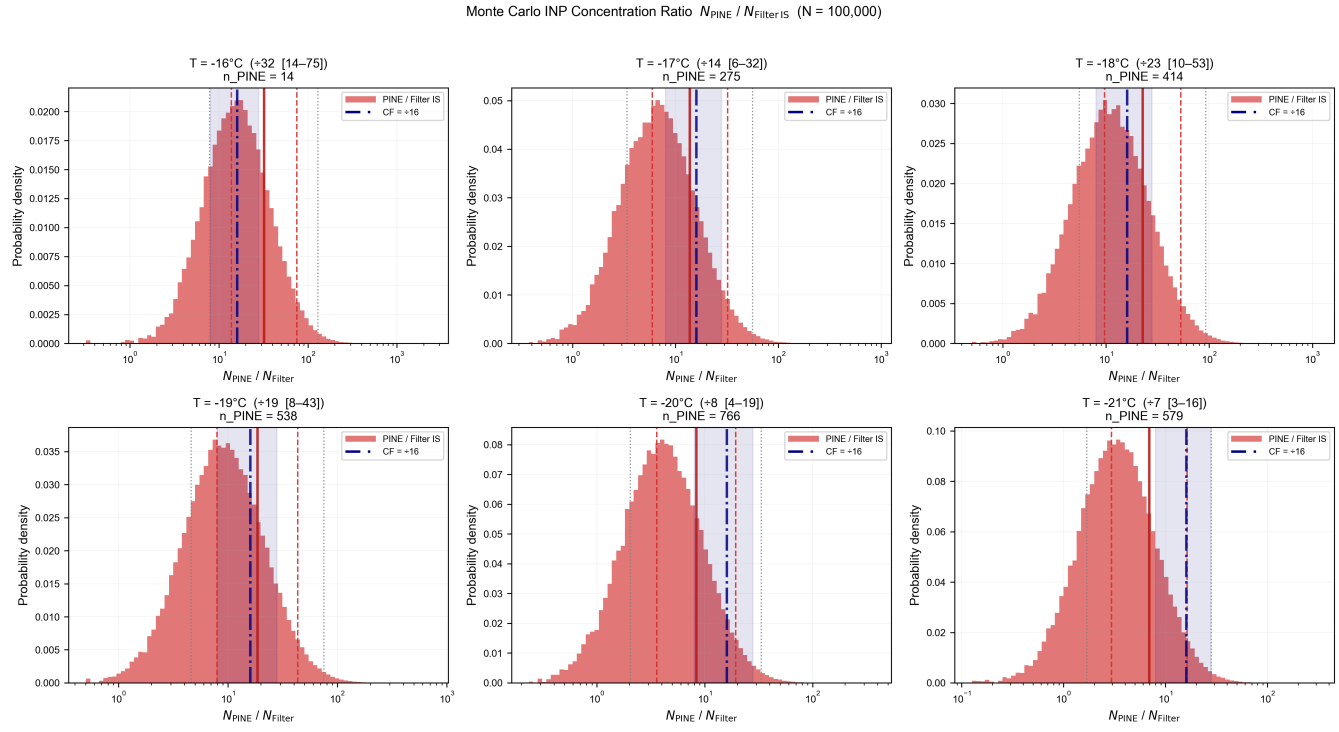

Figure A2. Monte Carlo distributions of the PINE/Filter IS INP concentration ratio at six temperatures (-16, -17, -18, -19, -20, $-21\,^{\circ}$C; $N = 100{,}000$ realisations per panel). The warmest bins are limited by the number of clean expansion runs; $-16\,^{\circ}$C ($n = 14$) is the warmest bin retaining sufficient runs for a stable estimate (the $-19\,^{\circ}$C value in the ship QC is a conditional warm-temperature spike-detection threshold, not an analysis cap). Solid vertical lines indicate the median; dashed lines mark the 16th and 84th percentiles (68 % percentile interval). The blue dash-dotted line marks the CF $= 16$ for reference; the MC envelopes bracket this value across the analysis range.